END
DATE
FILMED

1 -78

DDC

AD A047805

RE-548

INVESTIGATION OF VTOL UPWASH
FLOWS FORMED BY
TWO IMPINGING JETS
November 1977

12

DDC
RECEIVED
DEC 20 1977
E

RESEARCH DEPARTMENT

GRUMMAN AEROSPACE CORPORATION
BETHPAGE NEW YORK

REPORT DOCUMENTATION PAGE		READ INSTRUCTIONS BEFORE COMPLETING FORM
1. REPORT NUMBER RE-548	2. GOVT ACCESSION NO.	3. RECIPIENT'S CATALOG NUMBER
4. TITLE (and Subtitle) Investigation of VTOL upwash Flows Formed by Two Impinging Jets		5. TYPE OF REPORT & PERIOD COVERED Research
		6. PERFORMING ORG. REPORT NUMBER XXXXXX RE-548
7. AUTHOR(s) Richard C. Jenkins and William G. Hill Jr.		8. CONTRACT OR GRANT NUMBER(s)
9. PERFORMING ORGANIZATION NAME AND ADDRESS Grumman Aerospace Corporation Research Department Bethpage, New York 11714		10. PROGRAM ELEMENT, PROJECT, TASK AREA & WORK UNIT NUMBERS
11. CONTROLLING OFFICE NAME AND ADDRESS		12. REPORT DATE November 1977
		13. NUMBER OF PAGES 75
14. MONITORING AGENCY NAME & ADDRESS(if different from Controlling Office)		15. SECURITY CLASS. (of this report) unclassified
		15a. DECLASSIFICATION/DOWNGRADING SCHEDULE

16. DISTRIBUTION STATEMENT (of this Report)

Approved for public release; distribution unlimited

17. DISTRIBUTION STATEMENT (of the abstract entered in Block 20, if different from Report)

D D C
RECEIVED
DEC 20 1977
E

18. SUPPLEMENTARY NOTES

19. KEY WORDS (Continue on reverse side if necessary and identify by block number)

20. ABSTRACT (Continue on reverse side if necessary and identify by block number)

This report presents results of an experimental investigation of the complex flows that occur under a VTOL vehicle operating near the ground. Using the experimental results, we have modeled the effects of geometric and operating parameters on the upwash flow produced by ground impingement of two parallel subsonic jets. We have subdivided this flow into separate, modular elements: jet impingement, wall jet behavior, stagnation line formation, and upwash flow field properties. Models have been developed and evaluated for each of these elements. These models can be used in numerical computation methods

DD FORM 1473 EDITION OF 1 NOV 65 IS OBSOLETE
1 JAN 73
S/N 0102-014-6601

has been subdivided

have been modeled

20. that have been developed to predict such ground effects as suckdown and upwash lift on VTOL aircraft. Parameters included in this investigation were jet velocity, distance from the ground, separation distance between jets, relative jet strength, impingement angle, and nozzle diameter. Properties of the upwash were determined by local flow measurements above the ground and by ground plane measurements of surface pressure and oil flow patterns. Our data verified the radial velocity decay rate reported by other investigators for wall jets formed by single incident jets and established the velocity decay rate in the upwash flow produced by two jets with normal incidence. Models are presented for computing the effects on the upwash of jet strength ratio and impingement angle. Predictions of models are compared to measurements of upwash inclination angle and surface stagnation line location and shape.

Grumman Research Department Report RE-548

INVESTIGATION OF VTOL UPWASH FLOWS
FORMED BY TWO IMPINGING JETS

by

Richard C. Jenkins

and

William G. Hill, Jr.

Fluid Dynamics

November 1977

87 p.

Approved by: *Richard Scheuing*
Richard A. Scheuing
Director of Research

D D C
RECEIVED
DEC 21 1977

406165

ABSTRACT

This report presents results of an experimental investigation
of the complex flows that occur under a VTOL vehicle operating
near the ground. Using the experimental results, we have modeled
the effects of geometric and operating parameters on the upwash
flow produced by ground impingement of two parallel subsonic
jets. We have subdivided this flow into separate, modular
elements: jet impingement, wall jet behavior, stagnation line
formation, and upwash flow field properties. Models have been
developed and evaluated for each of these elements. These models
can be used in numerical computation methods that have been
developed to predict such ground effects as suckdown and upwash
lift on VTOL aircraft. Parameters included in this investigation
were jet velocity, distance from the ground, separation distance
between jets, relative jet strength, impingement angle, and
nozzle diameter. Properties of the upwash were determined by
local flow measurements above the ground and by ground plane
measurements of surface pressure and oil flow patterns. Our
data verified the radial velocity decay rate reported by other
investigators for wall jets formed by single incident jets and
established the velocity decay rate in the upwash flow produced
by two jets with normal incidence. Models are presented for
computing the effects on the upwash of jet strength ratio and
impingement angle. Predictions of these models are compared to
measurements of upwash inclination angle and surface stagnation
line location and shape.

iii

TABLE OF CONTENTS

LIST OF ILLUSTRATIONS

LIST OF SYMBOLS

d jet nozzle diameter

e separation distance between jet centerlines

h distance between nozzle exit plane and ground plane

h' distance from ground plane normal to surface

h'' distance from ground plane along center of upwash

h_c distance from midpoint between jet impact points to nozzle exit plane

K constant that depends on diameter ratio of unequal jets

L function described by Eq. (13)

L_o constant defined by Eq. (8)

m local flow momentum

p local static or surface pressure

q local dynamic pressure

q_j dynamic pressure at jet exit

r radial distance from jet centerline

r' radial distance along ground plane from wall jet effective origin

r_s radial distance along ground plane to stagnation line

u local flow velocity

u_o maximum upwash velocity at a given value of h' for $y = 0$

u_{ro} maximum upwash velocity at the ground surface for $y = 0$

u_r upwash velocity above ground computed from stagnation line surface pressure

u_m maximum wall jet velocity in a local velocity profile above ground

u_φ radial velocity of wall jet formed by inclined incident jet

u_{180} radial velocity of wall jet for $\phi = 180$ degrees

W empirical constant used to evaluate u_φ

x distance downstream of nozzle exit plane

y distance normal to midpoint between nozzle centerlines measured in plane containing both nozzle centerlines

y' distance along ground plane from midpoint between nozzle centerlines measured in plane containing both nozzle centerlines

y'_o displacement of stagnation line along ground plane from midpoint between nozzle centerlines.

y'_c displacement of maximum surface pressure point along ground plane from impact point of an inclined jet

z distance from midpoint between nozzle centerlines, measured normal to x and y

θ inclination of upwash path relative to normal to ground surface

ϕ azimuthal angle

σ_J jet inclination angle relative to ground plane

Subscripts

1   conditions in stronger of two wall jets, also conditions in wall jets formed by closer of two inclined jets

2   conditions in weaker of two wall jets, also conditions in wall jets formed by further of two inclined jets

j   properties in incident jet at nozzle exit plane

1. INTRODUCTION

Existing VTOL aircraft are severely restricted in performance, sacrificing either payload or range in order to achieve VTO capability. This restriction is traceable to the additional weight associated with thrust vectoring hardware for the primary propulsion system and separate lift engines and to aerodynamic problems that are peculiar to VTOL aircraft design. These latter problems are primarily caused by jet-induced effects that are basically different when the aircraft is close to or far from the ground (Ref. 1). Out-of-ground effects involve lift losses that are associated with the entrainment of ambient air by downward-directed jets and the free stream flow field distortions produced by the exhausts as the aircraft begins transition to horizontal flight. In-ground effects include stronger lift losses incurred by enhanced entrainment close to the ground (suckdown), engine thrust loss caused by inlet ingestion of hot exhaust gases, and fountain impingement on the aircraft underside. A review of past investigations of VTOL flow fields is given in Ref. 2.

VTOL aircraft performance is more strongly influenced by propulsion-induced effects than CTOL designs because of the strong interaction between the exhaust flow and the vehicle environment. Ground impingement of multiple jet exhausts from a VTOL aircraft produces a complex flow field that is not amenable to direct calculation by conventional aerodynamic analysis. Prediction of VTOL aerodynamic performance characteristics requires an analysis that can account for many different flow field processes that are dominated by turbulent mixing and entrainment of ambient air. Reference 3 describes the development

1

of techniques used by Grumman to predict pressure distributions and aerodynamic characteristics for V/STOL aircraft operating both in and out of ground effect. This method employs a modular approach to predict both the jet ground plane interaction effects on the aircraft and transitional flight parameters. Figure 1 illustrates the different flow field processes that are treated as separate modules in the analysis. Each of these modules, such as ground impingement, fountain formation, and inlet ingestion, were modeled from existing experimental data and combined into a computer program that predicts aircraft performance in ground effect. The modular nature of the analysis facilitates improvement of computer predictions as more detailed experimental data becomes available to improve component modeling.

As shown in Figure 1, each of the impinging jet exhausts from a VTOL aircraft produces on the ground a flow called a wall jet that turns parallel to the ground. A dominant process in ground effect is the formation of upward flows by colliding wall jets; collision of two wall jets forms a broad fan-shaped flow called an upwash. A concentrated, jet-like flow called a fountain can exist when three (or more) upwash lines intersect. The location, direction, and intensity of the fountains depend on the upwash flows that form between pairs of adjacent jets. An understanding of upwash behavior between two impinging jets is a necessary first step in modeling the more complex multiple-jet ground plane interaction.

This investigation conducted experiments required to evaluate methods of predicting properties of the upwash flow produced by dual jet impingement. Our approach for modeling the upwash was to express its location, shape, and direction close to the ground in terms of wall jet properties and to use existing models that
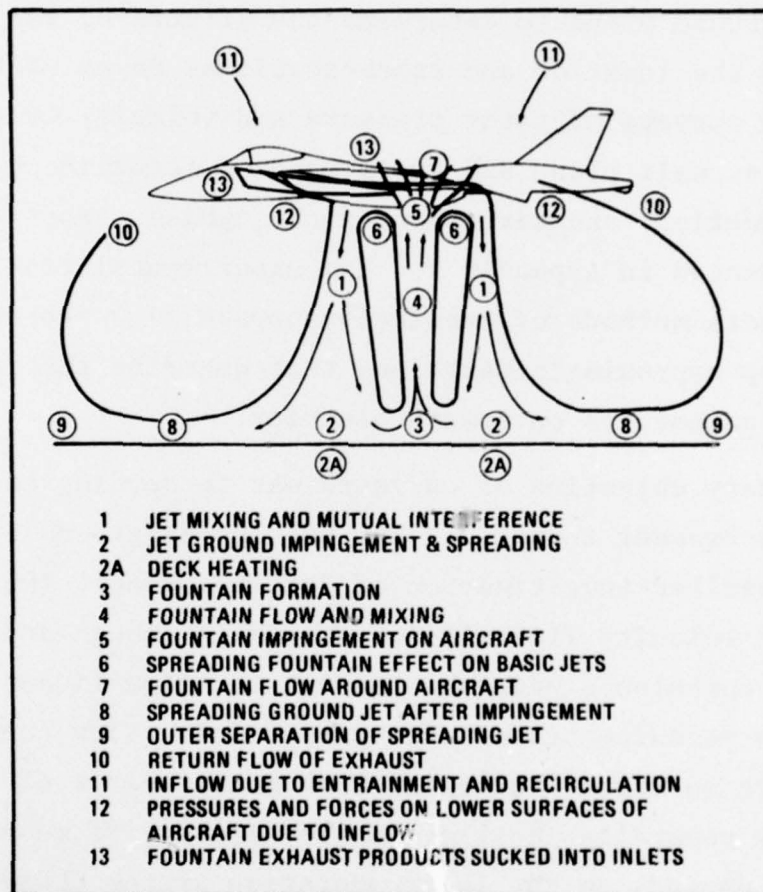
2

1	JET MIXING AND MUTUAL INTERFERENCE
2	JET GROUND IMPINGEMENT & SPREADING
2A	DECK HEATING
3	FOUNTAIN FORMATION
4	FOUNTAIN FLOW AND MIXING
5	FOUNTAIN IMPINGEMENT ON AIRCRAFT
6	SPREADING FOUNTAIN EFFECT ON BASIC JETS
7	FOUNTAIN FLOW AROUND AIRCRAFT
8	SPREADING GROUND JET AFTER IMPINGEMENT
9	OUTER SEPARATION OF SPREADING JET
10	RETURN FLOW OF EXHAUST
11	INFLOW DUE TO ENTRAINMENT AND RECIRCULATION
12	PRESSURES AND FORCES ON LOWER SURFACES OF AIRCRAFT DUE TO INFLOW
13	FOUNTAIN EXHAUST PRODUCTS SUCKED INTO INLETS

Fig. 1 VTOL Ground Interaction Flow Field

3

describe wall jet behavior to specify wall jet properties in terms of incident jet conditions. Incident jet parameters included in this investigation were the size of the nozzles, the spacing between them, relative jet strength, ground plane distance and jet impingement angle.

Measurements of surface pressure and oil flow patterns were made on the ground plane to determine the effects of the above parameters on the location and cross-sectional shape of the upwash fan. Spatial surveys of pitot pressure and velocity were taken between the jet exit plane and the ground to determine the intensity, location, and direction of the upwash. Most of these data are presented in Appendix A. The experimental results were used to evaluate methods of predicting upwash flow properties and to develop approximate relations that describe the influence of the above parameters on upwash behavior.

A secondary objective of our work was to develop and evaluate different measurement techniques for use in jet-ground interaction flows. Our earlier investigation of jet impingement (Ref. 4) revealed that velocity fluctuations were high enough and the scale of the turbulence was large enough for significant error to be present in measurements of flow properties. Flow conditions in the upwash are so highly turbulent that measurements of turbulence intensity are generally invalid and the accuracy of mean velocity measurements depends on the instrumentation system chosen. Appendix B describes our instrumentation techniques and the effects of flow field turbulence on measurement accuracy.

4

2. EXPERIMENTAL EQUIPMENT

Figure 2 shows one of the air supplies used to produce the subsonic free jets used in this work. This supply was a low turbulence level settling chamber that was driven by a 7-1/2 hp motor and centrifugal fan. Low turbulence levels (nominally $u'/U_j = 0.001$ at the nozzle exit) were obtained by using a honeycomb flow straightener and turbulence damping screens downstream of the diffuser. Jet velocity was varied by obstructing the fan inlet. A second air supply, similar in construction but smaller, was used primarily to obtain oil flow patterns on a horizontal ground plane.

The nozzles were either one- or two-inch i.d. thin-wall pipes that were seven inches long. Each nozzle had an elliptical entrance contour and was mounted flush with the inner settling chamber wall. Either 0.010- or 0.020-inch-thick trip rings were located just downstream of the entrance to provide a turbulent boundary layer. All experiments were conducted without any simulated fuselage structure near the nozzle exit plane (Figure 3) that would deflect the upwash flow and affect nozzle exit conditions.

Nozzle exit velocities were varied over the 150-350 ft/sec range. Because all of our dual jet configurations were run with both nozzles mounted on a single air supply, exit velocities of any nozzle pair were equal. However, part of our work involved investigation of the ground interaction of two jets having different nozzle exit conditions. Such impingement flows were produced by nozzles having unequal diameters. The jet strength ratio (d_2/d_1) was defined as the parameter of interest for this work. The diameter of one of the jets was reduced by sliding
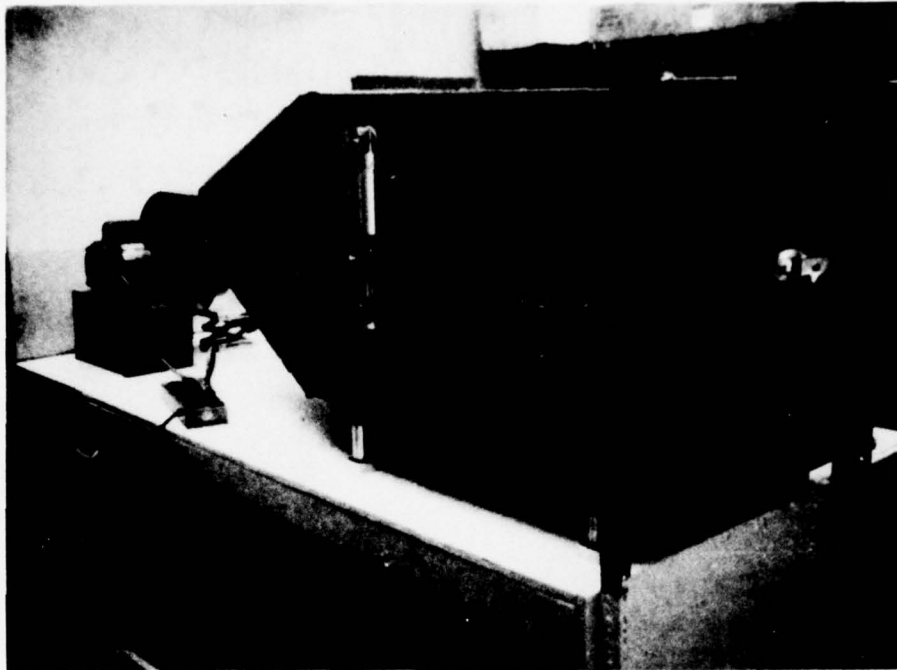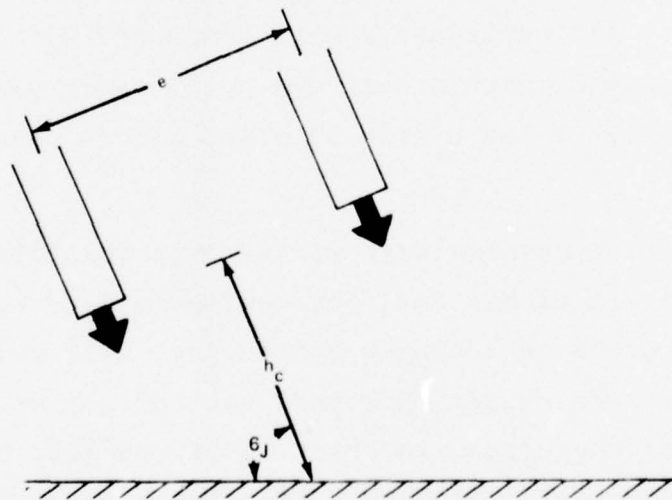
5

Fig. 2 Primary Test Facility

Fig. 3 Jet Impingement Flow Field

6

tapered inserts inside it, leaving at least several inches of constant diameter upstream of the exit. For most of the experiments with unequal strength jets the ground plane was normal to the incident jets.

Another parameter in this investigation was the distance h between the ground plane and the jet exits. For most tests h/d was between 2 and 6. For these conditions the ground plane was generally no further from the exit than the end of the core of the free jet. In some tests, however, with the ground plane inclined at large angles, the higher nozzle was necessarily located further than h/d = 6 from the ground plane to avoid having the lower nozzle closer than h/d = 2. Values of ground plane inclination angle σ_J were varied from 90° to 60°, as shown in Figure 3. The ground plane was inclined about an axis of rotation located midway between, and normal to, the nozzle centerlines. The distance between this axis of rotation and the nozzle exit plane (h_c) was held constant for different angles of inclination.

The ground plane used for most of this work was a 44 inch square plywood board mounted on a supporting structure that was displaced to vary h and rotated about a vertical axis to vary σ_J. The spacing between nozzle centerlines, e, was varied by changing the nozzle mounting flange on the settling chamber. The nozzle configuration for most of our work was e/d = 6.

Ground plane measurements consisted of surface pressure distributions along a line connecting jet impact points and measurements of stagnation line displacement and shape. Ground pressure profiles were obtained from a pressure tap in a thin plexiglas sheet that was slid across the plywood ground board, with a vernier scale used to measure pressure tap location.

7

Stagnation line measurements were taken from oil flow patterns on a two-foot-square metal sheet that was scribed with grid lines.

Two methods were used to measure local flow direction in the upwash formed by equal strength jets impinging normal to the ground. An array of small flags, supported on a ladder-like structure as shown in Figure 4, were photographed for angular measurement. In addition, direction-sensitive hot film probes were used to check data obtained from the flag array. A comparison of the data obtained using these two techniques is presented in Appendix B.

Pitot probe measurements were made in the upwash with two different traverse arrangements. Figure 5 shows a three-dimensional traverse mechanism that was used to obtain pitot pressure and velocity profiles when operating with normal jet impingement. For inclined jet impingement we used a probe traverse that was attached to the ground plane. Pitot probes were 1/8-inch o.d. steel tubes cut off to a flat end. We chose thin-wall tubing in order to make measurements less dependent on fluctuations of local flow angle (Ref. 5). A Validyne model CD15 transducer was used to obtain pressure measurements, which were time-averaged for digital display.

Velocity measurements were made in the upwash with a hot film anemometer, but the accuracy of this data was strongly affected by high turbulence levels, which are a dominant characteristic of this type of flow field. These results are described in Appendix B, which presents a more complete description of measurement techniques used to obtain local flow properties in the upwash.
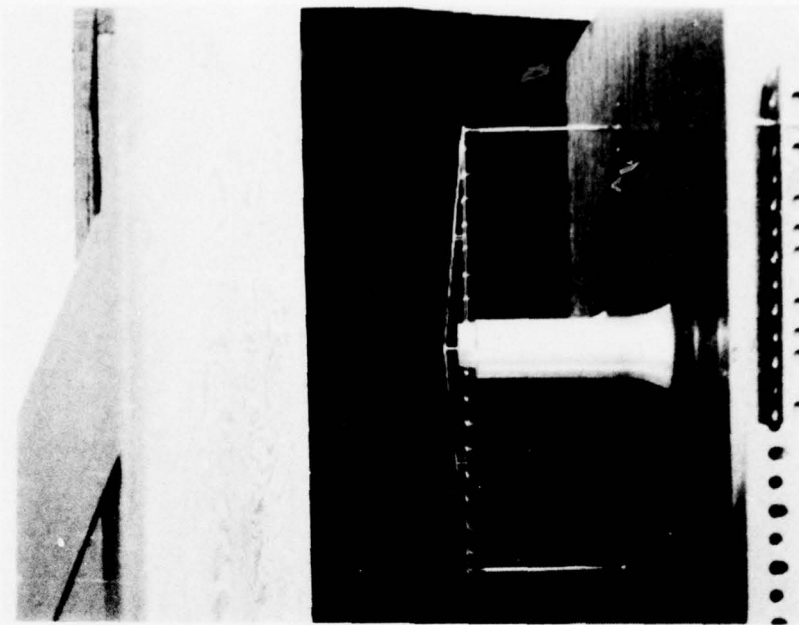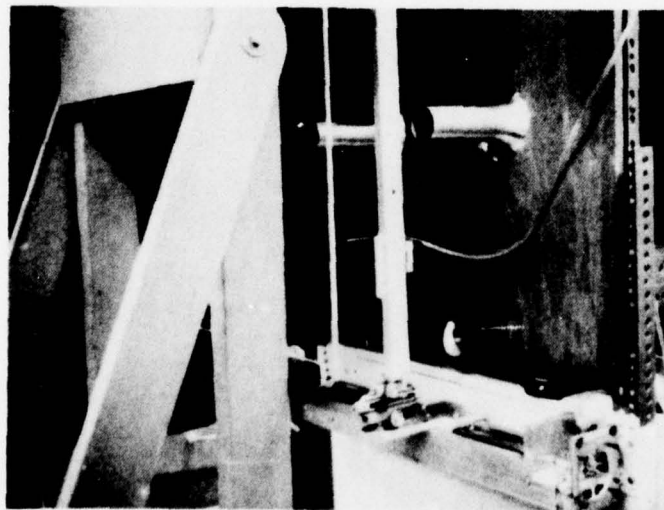
8

Fig. 4 Flag Array Immersed in Upwash

Fig. 5 Probe Traverse used for Upwash Surveys

3. PROPERTIES ON THE GROUND PLANE

Impingement of a single jet produces a radial flow on the ground that is influenced by entrainment and turbulent mixing with ambient air. For normal jet impingement, Glauert (Ref. 6) has shown that the radial decay in maximum velocity is proportional to $r^{-1.1}$ and that the thickness increases linearly with r. This model of wall jet behavior is valid far from the impingement point where the incident jet has undergone a transition to flow parallel to the wall. Donaldson and Snedeker (Ref. 7) noted that this result is valid at least over the Reynolds number range from 10^4 to 2×10^5 based on wall jet thickness. Because the wall jet velocity profiles exhibit approximate similarity, this model can be used to describe the radial decay of either the maximum velocity or the average velocity of the wall jet.

NORMAL IMPINGEMENT OF TWO PARALLEL JETS

Impingement of two parallel jets, such as these shown in Figure 6, produces two adjacent wall jets on the ground plane. Collision of these wall jets on the ground plane develops a flow directed away from the surface, called an upwash, that is illustrated in Figure 7. A stagnation line forms on the ground at the base of the upwash where the wall jets collide. The location and shape of the stagnation line depends on incident jet properties and on the geometric configuration. For incident jets of equal strength inclined normal to the surface, the stagnation line is straight and located midway between jet impact points.

The surface pressure at the stagnation line is dependent on local wall jet properties. Let p_m denote the surface pressure at the stagnation line and let u_m represent the maximum wall jet
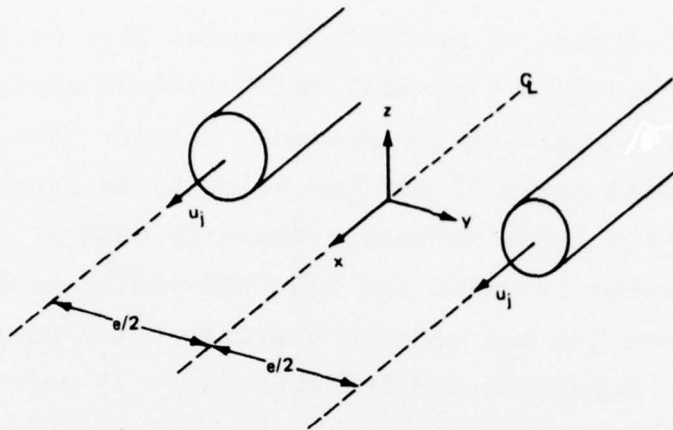
11
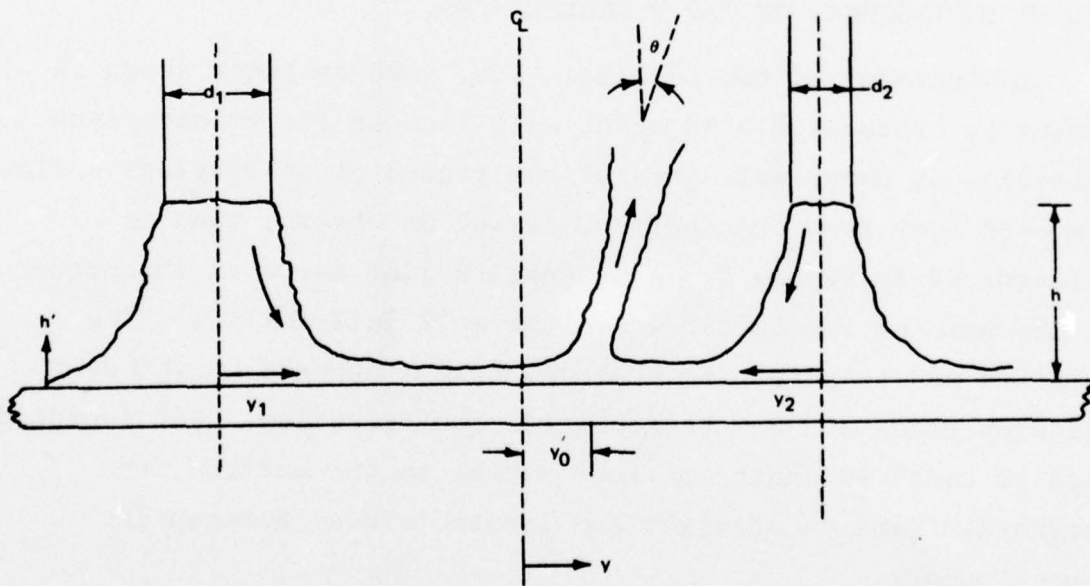
Fig. 6 Coordinate System For Free Jets

Fig. 7 Sketch of Unequal Jet Impingement

12

velocity that would exist at the stagnation line location if
the wall jet were undisturbed. If the wall jet comes to rest
at the stagnation line with no losses, then

$$\frac{(P_m - P_a)}{q_j} = \left(\frac{U_m}{U_j}\right)^2 \tag{1}$$

where q_j and u_j represent jet exit conditions and P_a is the
ambient pressure. The value of p_m cannot be predicted analytically
from incident jet conditions but must be measured experimentally
for a particular impingement configuration.

Figure 8 shows the surface pressure distribution along a
line between jet impact points for equal strength jets impinging
normal to the surface. The high pressure region at the stagnation
line is isolated from the impingement regions by a significant
distance over which the pressure is essentially equal to ambient
pressure. The maximum pressure on the stagnation line was not
affected by increasing the ground plane distance h/d from 2 to 3.
Increasing the jet separation e/d from 6 to 12 decreased the
maximum pressure on the stagnation line by a factor of 4.6 (see
sheet 2 of Figure A-1 in Appendix A). This pressure decrease is
consistent with Eq. (1) if we assume that the velocity decay
in the wall jets follow

$$\frac{u_m}{u_j} \sim \left(\frac{r}{d}\right)^{-1.1} \tag{2}$$

as found by Glauert.

When two parallel jets of unequal strength impinge normal
to a ground plane the stagnation line on the surface is displaced
by a distance y_o' from the midpoint between nozzle centerlines
toward the weaker jet. Displacement of the stagnation line can
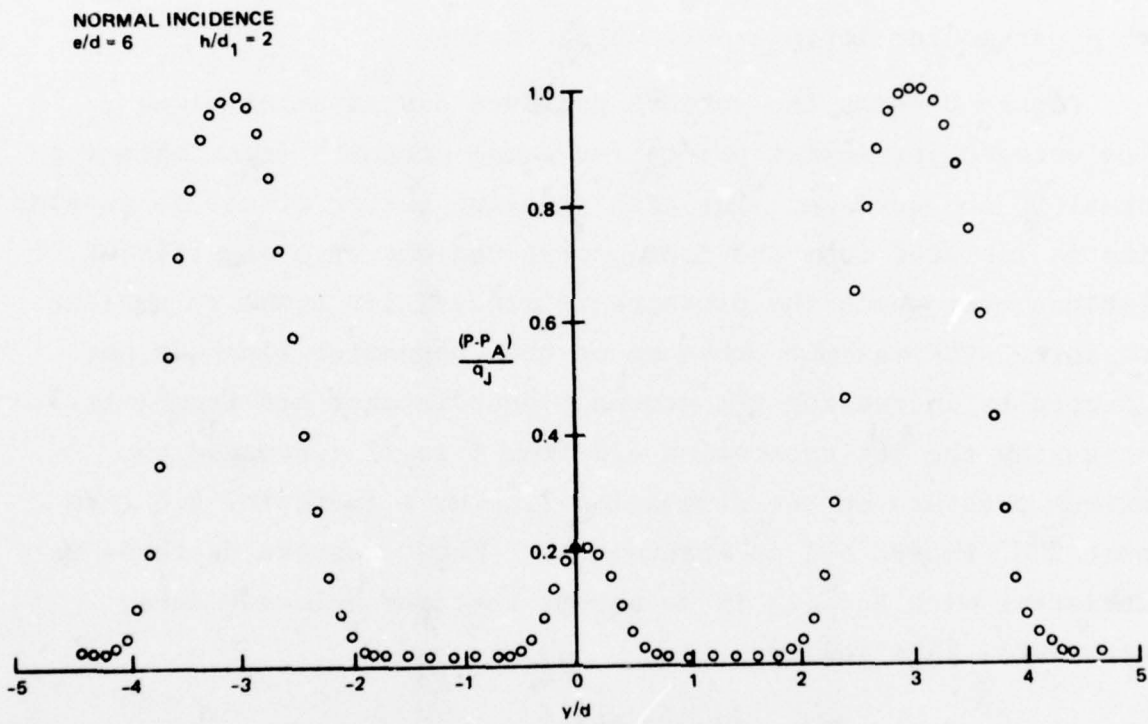be observed from ground pressure surveys such as that shown in

13

NORMAL INCIDENCE
e/d = 6   h/d$_1$ = 2

Fig. 8 Ground Plane Pressure Distribution for Equal Strength Jets

14

Figure 9. A symbol (filled circle) has been added to this plot
to indicate the stagnation line location determined from oil
flow studies. When the stagnation line is displaced toward the
weaker incident jet it is also curved towards the impact region
of the incident jet. Note that surface pressure below ambient
were found on the ground plane in a small region located between
the weaker jet and the upwash. Surface pressures lower than
ambient may develop because air entrainment into the weaker
incident jet, its wall jet, and the upwash takes place from a
region above the surface that is almost completely surrounded
by shear layers.

The magnitude of the stagnation line displacement can be
found from the condition that at the stagnation line the average
velocity of both wall jets must be the same. Let the subscript j
denote jet exit conditions and let the subscripts 1 and 2 denote
properties of the stronger and weaker jets, respectively. Then
the wall jet velocity ratio can be expressed in terms of the
jet exit velocities and diameters as

$$\frac{u_1}{u_2} = \frac{u_{j1}}{u_{j2}} \left(\frac{y_2}{y_1} \frac{d_{j1}}{d_{j2}} \right)^{1.1} \tag{3}$$

where y_1 and y_2 represent the distances between the stagnation
line and the stronger and weaker jet centerlines, respectively.
Since $u_1 = u_2$ at the stagnation line, and since our experiments
were run with $u_{j1} = u_{j2}$

$$\frac{y_2}{y_1} = \frac{d_{j2}}{d_{j1}} \tag{4}$$

In terms of nozzle separation distance e

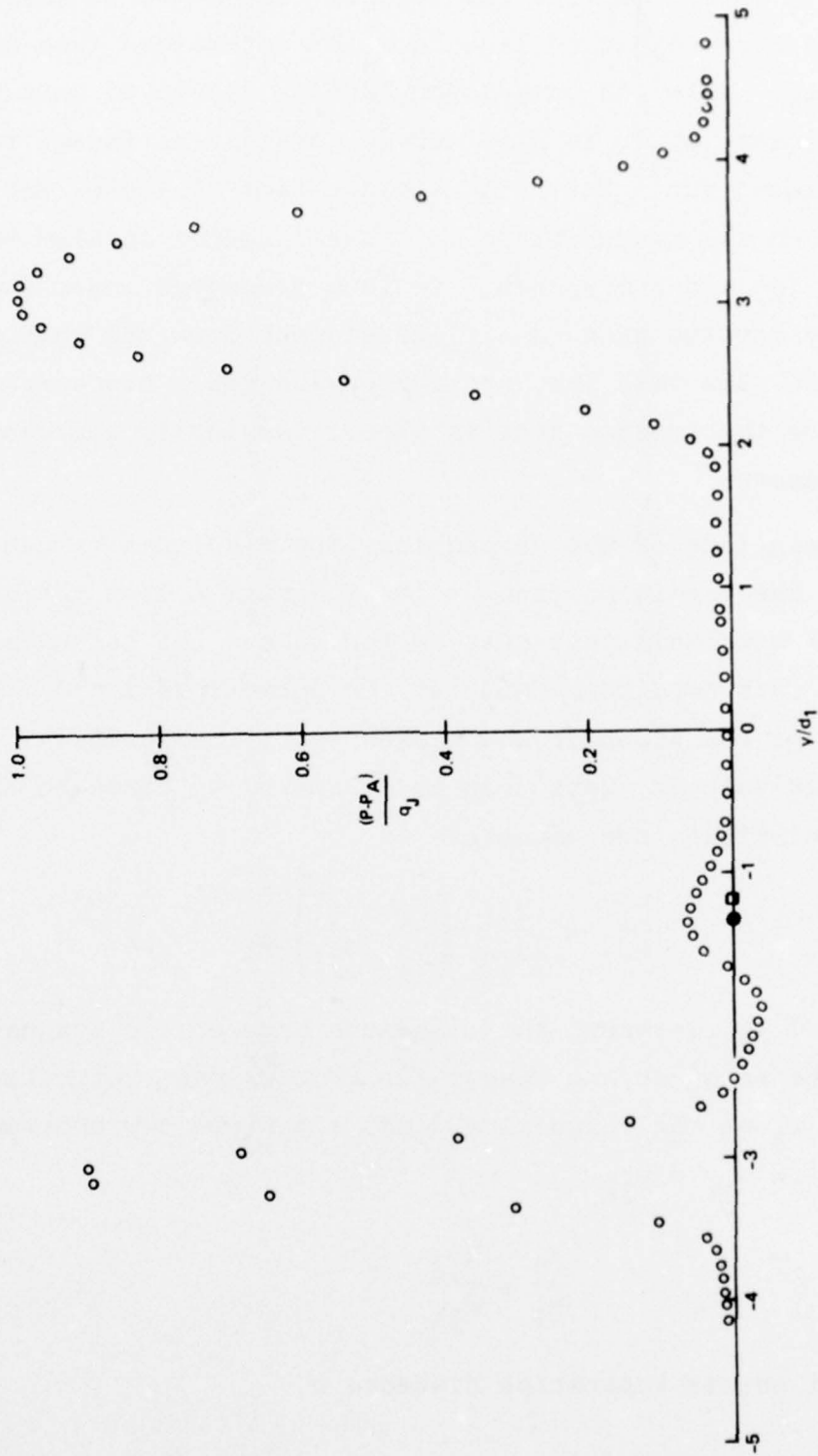$$y_1 = e/2 + y_o \qquad \text{and} \qquad y_2 = e/2 - y_o$$

15

Fig. 9 Ground Plane Pressure Distribution for Unequal Strength Jets

16

which yields

$$y_o = \frac{e}{2} \left[\frac{y_1/y_2 - 1}{y_1/y_2 + 1} \right]$$

Then the stagnation line displacement can be expressed in terms of nozzle diameter ratio as

$$y_o = \frac{e}{2} \left[\frac{d_{j1}/d_{j2} - 1}{d_{j1}/d_{j2} + 1} \right] \tag{5}$$

Equation (5) is shown plotted in Figure 10 where it is compared to measurements of stagnation line location that were obtained using oil flow techniques.

INCLINED JET IMPINGEMENT

Impingement of a single jet on an inclined ground plane produces a wall jet in which the flow properties depend on both radial distance and azimuthal orientation. Let ϕ be an angular measurement around the jet impact point on the ground plane, defining $\phi = 0$ as the orientation of maximum velocity on the ground plane. Donaldson and Snedeker (Ref. 7) have shown that for oblique jet impingement the maximum pressure point on the ground plane is displaced away from the jet centerline in the direction $\phi = 180^o$. Let this displacement distance be denoted by y_c'. This shifted stagnation point represents the effective origin of the wall jet flow that is described by the coordinates r' and ϕ, where the prime is used to denote distance along the inclined ground plane. The magnitude of y_c' depends on both jet inclination angle and distance from the jet exit to the ground.

When two parallel jets of equal strength impinge on a ground plane with angle σ_J, as shown in Figure 11, the stagnation line
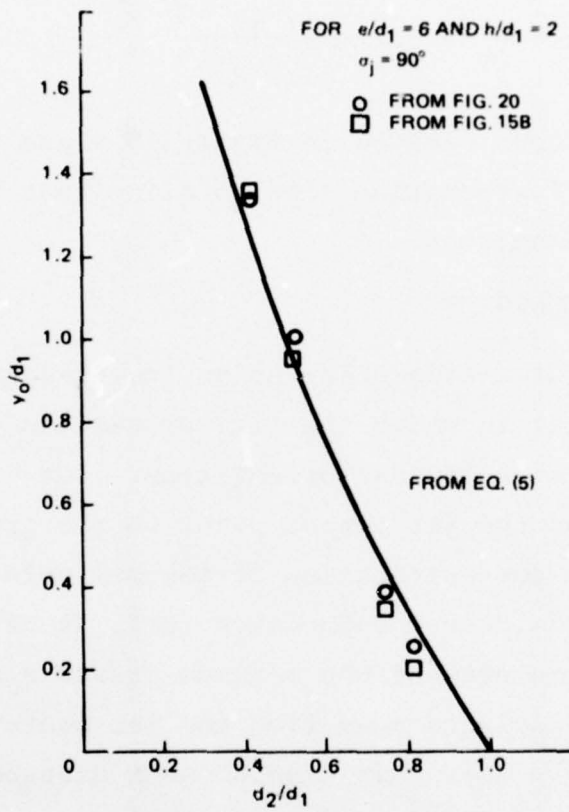
17

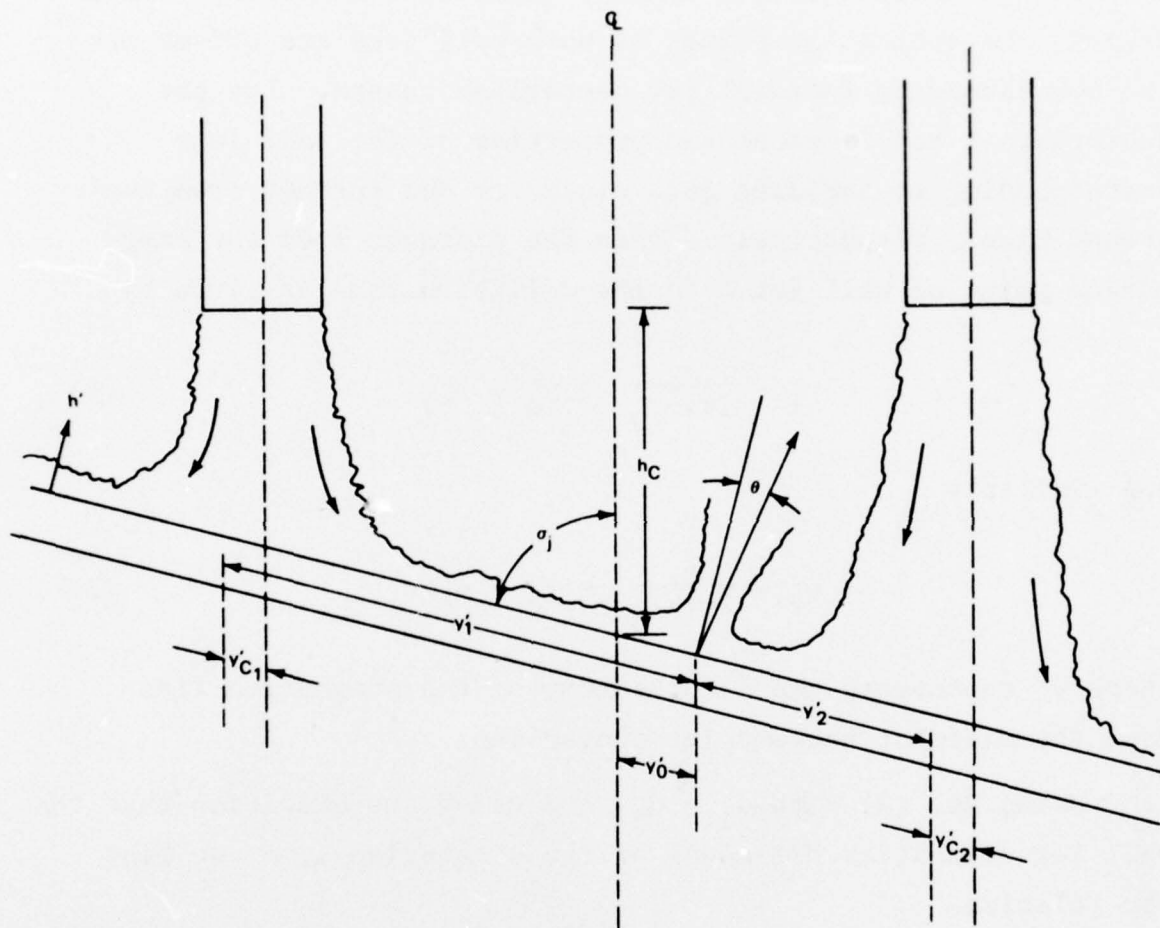**Fig. 10 Effect of Jet Strength Ratio on Stagnation Line Displacement**

18

Fig. 11 Sketch of Inclined Jet Impingement

19

on the ground plane is offset from the midpoint between jet centerlines by a distance y_o' because of two effects. First, the velocity in one of the wall jets as it approaches the midpoint is lower than the other because of the wall inclination. Second, the stagnation points of both wall jets are offset from the corresponding incident jet centerline points. Let the subscripts 1 and 2 denote the properties of the wall jets corresponding to incident jets closer to and further from the ground plane, respectively. Then the distance from the stagnation point of wall jet 1 to the collision line is given by

$$y_1' = \frac{e}{2\sin\sigma_J} + y_o' + y_{c1}' \tag{6}$$

and similarly

$$y_2' = \frac{e}{2\sin\sigma_J} - y_o' - y_{c2}' \tag{7}$$

where y_o' represents the displacement of the stagnation line from the midpoint between jet centerlines.

Using Eq. (3) with $d_1 = d_2$, and using the condition that the wall jet velocities are equal at the stagnation line, we find the relation

$$\frac{y_1'}{y_2'} = \left(\frac{u_{j1}}{u_{j2}}\right)^{1/1.1}$$

For application to inclined incident jets having $u_{j1} = u_{j2}$, the velocity ratio in the above relation must take into account the variation of wall jet velocity with ϕ. Since one wall jet approaches the stagnation line with $\phi = 180^o$ and the other with $\phi = 0$, the stagnation line displacement is dependent on the wall jet strength ratio

20

$$\frac{u_{\phi=0}}{u_{\phi=180}}$$

Values of this velocity ratio have been measured on a single jet at different impingement angles by other investigators. We define

$$L_o \equiv \frac{y'_1}{y'_2} = \left[\frac{(u_1)_{\phi=0}}{(u_1)_{\phi=180}}\right]^{1/1.1} \qquad (8)$$
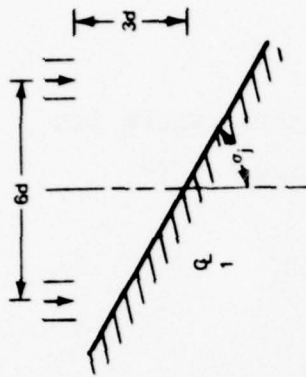
Combining Eqs. (6), (7), and (8)

$$y'_o = \frac{e}{2\sin\sigma_J}\left(\frac{L_o-1}{L_o+1}\right) - \left(\frac{y'_{c1}+L_o\,y'_{c2}}{1+L_o}\right) \qquad (9)$$

For two parallel jets inclined at an angle σ_J, h/d varies for each nozzle as σ_J is changed. The data presented in Reference 7 show that both y'_c and L_o are functions of h/d as well as σ_J, and the influence of h/d is quite strong. While Reference 7 presents the most complete investigation of inclined jet impingement that is available, it does not provide sufficient data to evaluate the effects of h/d on either y'_c or L_o because the increments in h/d chosen were too large.

Therefore to apply Eq. (9) we must neglect effects of h/d. This approximation yields $y'_{c1} = y'_{c2} = y'_c$ since σ_J is the same for each incident jet, and Eq. (9) reduces to

$$y'_o = \frac{e}{2\sin\sigma_J}\left(\frac{L_o-1}{L_o+1}\right) - y'_c \qquad (10)$$

Figure 12 shows the ground pressure distribution along a line connecting jet impact points for equal strength jets impinging on an inclined surface. Note that the maximum pressure opposite

21

Fig. 12 Ground Plane Pressure Distribution for Inclined Jets

OIL LINE
EXTRAPOLATED UPWASH

EQUAL JETS $\sigma_i = 60°$
$e/d = 6$ $h_c/d = 3$

$\frac{(P-P_A)}{q_J}$

y'/d

each jet is displaced from the impact centerline. Effects of h/d
on the two jet impact pressure profiles that are evident in this
plot include differences in the amount of maximum pressure dis-
placement, the maximum pressure levels, and the amount of profile
distortion from symmetry. A symbol has been added to this plot to
indicate the stagnation line location determined from oil flow
studies.

Measurements of stagnation line location were taken for jet
inclination angles of 80°, 70°, and 60°. Figure 13 shows this
data compared to the variation of y_o' predicted by Eq. (10). To
apply Eq. (10), we used the following values of L_o and y_c' that
were taken from data presented for single jet impingement by
Donaldson and Snedeker:

σ_J	L_o	y_c'/d
80°	1.38	.153
70°	2.07	.307
60°	3.18	.46

STAGNATION LINE SHAPE

For unequal strength jets impinging normal to the ground
plane the upwash line is displaced toward, and concave toward,
the weaker jet, as shown in Figure 14. The shape of the
stagnation line on the ground plane can be determined by
assuming that along this line the velocity components normal to
the stagnation line in each wall jet must be equal. This
assumption yields an expression for the slope of the stagnation
line that requires numerical integration to determine the exact
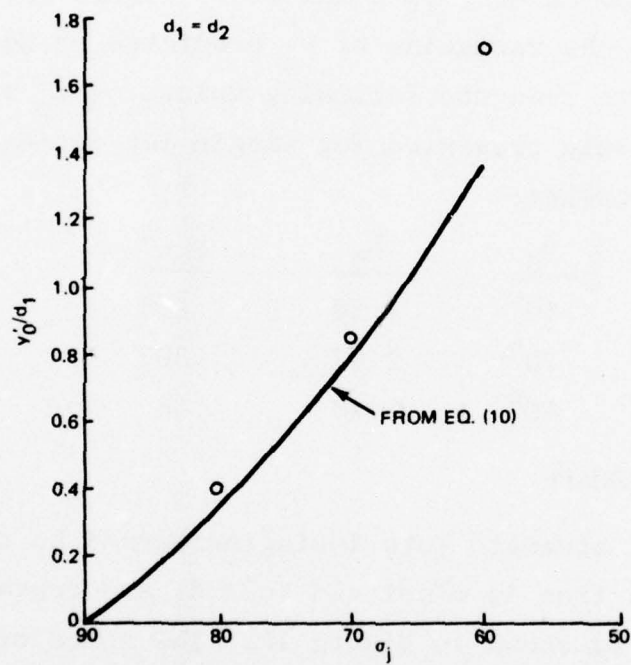shape of the line.

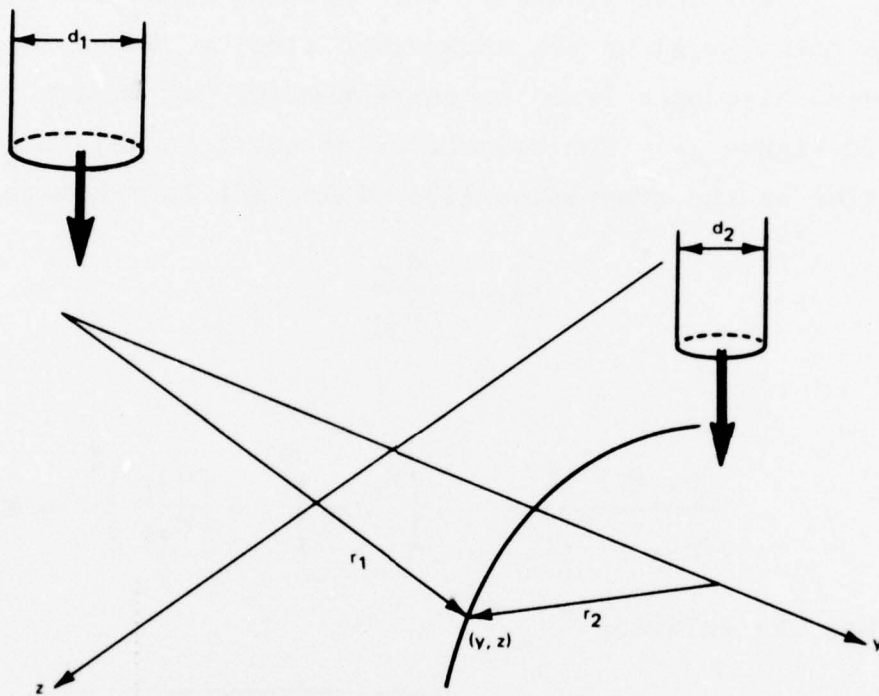Fig. 13 Effect of Jet Inclination on Stagnation Line Displacement

24

Fig. 14 Stagnation Line on Ground Plane

To get an approximate expression for the stagnation line shape we will assume that radial velocity components are equal along the stagnation line (rather than the velocity components normal to the stagnation line). At the stagnation line the ratio of radial wall jet velocities is given by a relation similar to Eq. (3), except that y_1 and y_2 are replaced by r_1 and r_2. For a given point (y,z) on the stagnation line, r_1 and r_2 represent the radial distances from the corresponding jet impact points as shown in Figure 14. The assumption of equal radial wall jet velocities on the stagnation line yields the approximate relation

$$\frac{r_1}{r_2} = \frac{d_{j2}}{d_{j1}}$$

Then

$$\frac{(e_{/2}+y)^2+z^2}{(e_{/2}-y)^2+z^2} = \left(r_1/r_2\right)^2 = \left(\frac{d_{j1}}{d_{j2}}\right)^2 = K$$

which has the solution

$$y = \frac{e}{2}\left(\frac{K+1}{K-1}\right) - \sqrt{\left(\frac{e}{2}\right)^2\left[\frac{4K}{(K-1)^2}\right] - z^2} \qquad (11)$$

Figure 15b shows stagnation line shapes measured from oil flow patterns compared to solid curves that were obtained from Eq. (11). The dashed curves shown in this figure were developed by a computer prediction technique, described in Ref. 2, that balances normal wall jet velocity components along the stagnation line. This comparison shows that Eq. (11) can be used to locate approximately the central region of the upwash.

To find the stagnation line shape for equal strength jets impinging on an inclined ground plane we will again assume that
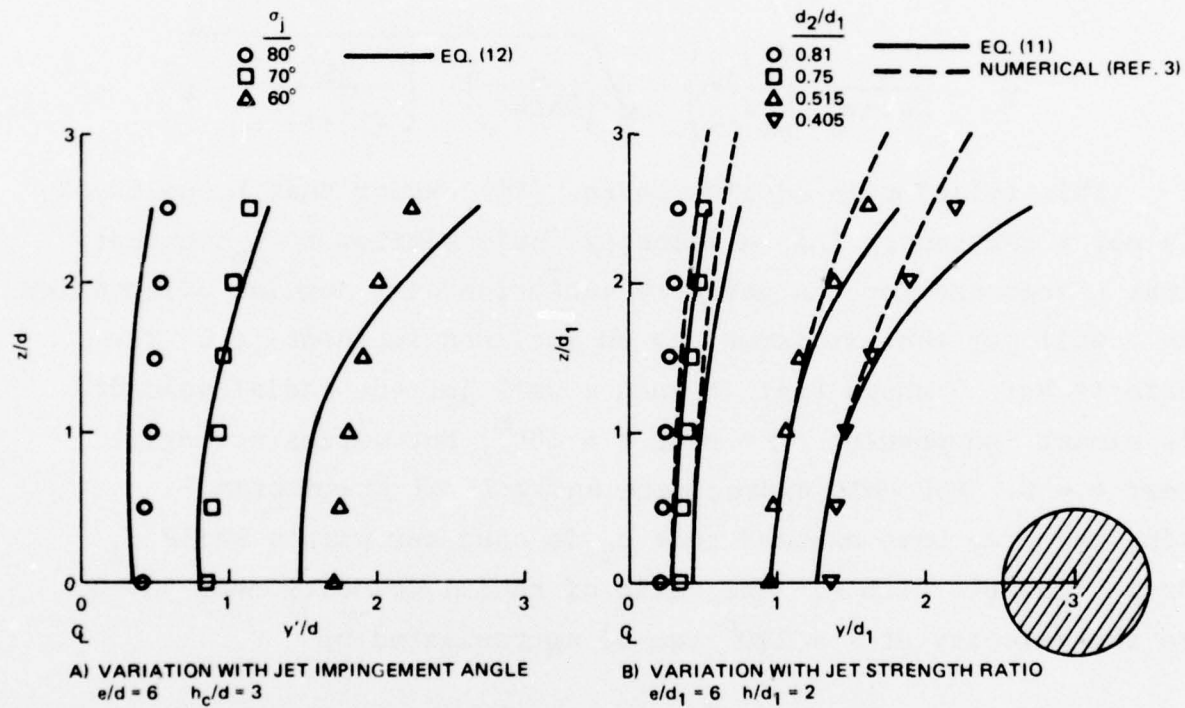
26

Fig. 15 Effects of Impingement Conditions on Stagnation Line Shape

radial wall jet velocity components are equal along the stagnation line. At a given point (z, y') on the ground plane, if r_1' and r_2' are radial distances along the ground plane to the corresponding wall jet origins, then using Eq. (8)

$$\frac{\left(\frac{e}{2\sin\sigma_J} + y' + y_c'\right)^2 + z^2}{\left(\frac{e}{2\sin\sigma_J} - y' - y_c'\right)^2 + z^2} = \left(\frac{r_1'}{r_2'}\right)^2 \equiv L^2$$

and

$$y' = \frac{e}{2\sin\sigma_J}\left(\frac{L^2+1}{L^2-1}\right) - \sqrt{\left(\frac{e}{2\sin\sigma_J}\right)^2\left[\frac{4L^2}{(L^2-1)^2}\right] - z^2} \; - y_c' \quad (12)$$

This relation is similar to Eq. (11) except that L, unlike K, is not a constant. L is a velocity ratio similar to L_0, except that L accounts for the velocity variation with angular orientation in a wall jet that is formed by an inclined incident jet. The data in Ref. 7 shows that in such a wall jet the radial velocity is almost independent of ϕ near $\phi = 180^o$, but varies strongly near $\phi = 0$. For this approximate analysis of stagnation line shape we have assumed that u_2 is constant with ϕ while u_1 drops linearly with ϕ. The ratio of radial velocity near $\phi = 0$ to the velocity at $\phi = 180^o$ can be approximated by

$$\frac{u_\phi}{u_{\phi=180}} = 1 - \left(\frac{\phi}{90}\right) W$$

where from Reference 7, W = 0.2, 0.3, and 0.5 for $\sigma_J = 80^o$, 70°, and 60°, respectively.

As a further approximation, we express ϕ in terms of z as

$$\phi \approx \tan^{-1}\left(\frac{z}{e/2}\right)$$

Then for a given value of σ_J, L is related to the constant L_o by

$$L = L_o \left\{ \left[1-W \left[\frac{\tan^{-1} \frac{2z}{e}}{90} \right] \right] \right\}^{1/1.1} \tag{13}$$

The curves shown in Figure 15a were obtained from Eqs. (12) and (13) using the values of W cited above. Comparison with the data shows that the central upwash region can be located without having to develop a more exact computer solution.

29

4. FLOW PROPERTIES IN THE UPWASH

EQUAL STRENGTH JETS, GROUND PLANE NORMAL

In this symmetric case the local flow direction in the upwash should be relatively independent of nozzle exhaust velocity, at least close to the ground plane where the effects of turbulent mixing on mean flow velocity are not dominant. The outward wall jet flow from each jet impact point is radial. To model the local flow direction in the upwash we have assumed that the radial flow pattern in the wall jets continues into the upwash. This flow model was proposed in Ref. 8. Then along the stagnation line the upwash velocity components normal to and parallel to the stagnation line can be found from wall jet conditions. According to this model the local upwash flow direction should be dependent only on e/d.

Local flow direction in the upwash formed between equal strength jets inclined normal to the ground was obtained by supporting an array of 17 flags in the plane $y = 0$. These flags were stiff paper rectangles, sized 0.4 by 0.7 inches and spaced one inch apart. They were mounted on a ladder-shaped wire support, as shown in Figure 5, so that each flag could pivot freely in the z-direction. Measurements of local flow direction were taken directly from such photographs as that shown in Figure 5. Data were obtained at different axial stations for h/d = 2, 4, and 6 with nozzle spacing e/d = 6. Additional data were taken with e/d = 3 and 9 for h/d = 4 only. Data obtained for one configuration are shown in Figure 16, in which short dashes are used to represent local flow direction. We show data only for positive values of z on this plot. Each dash represents the average value of measurements obtained at positive and negative
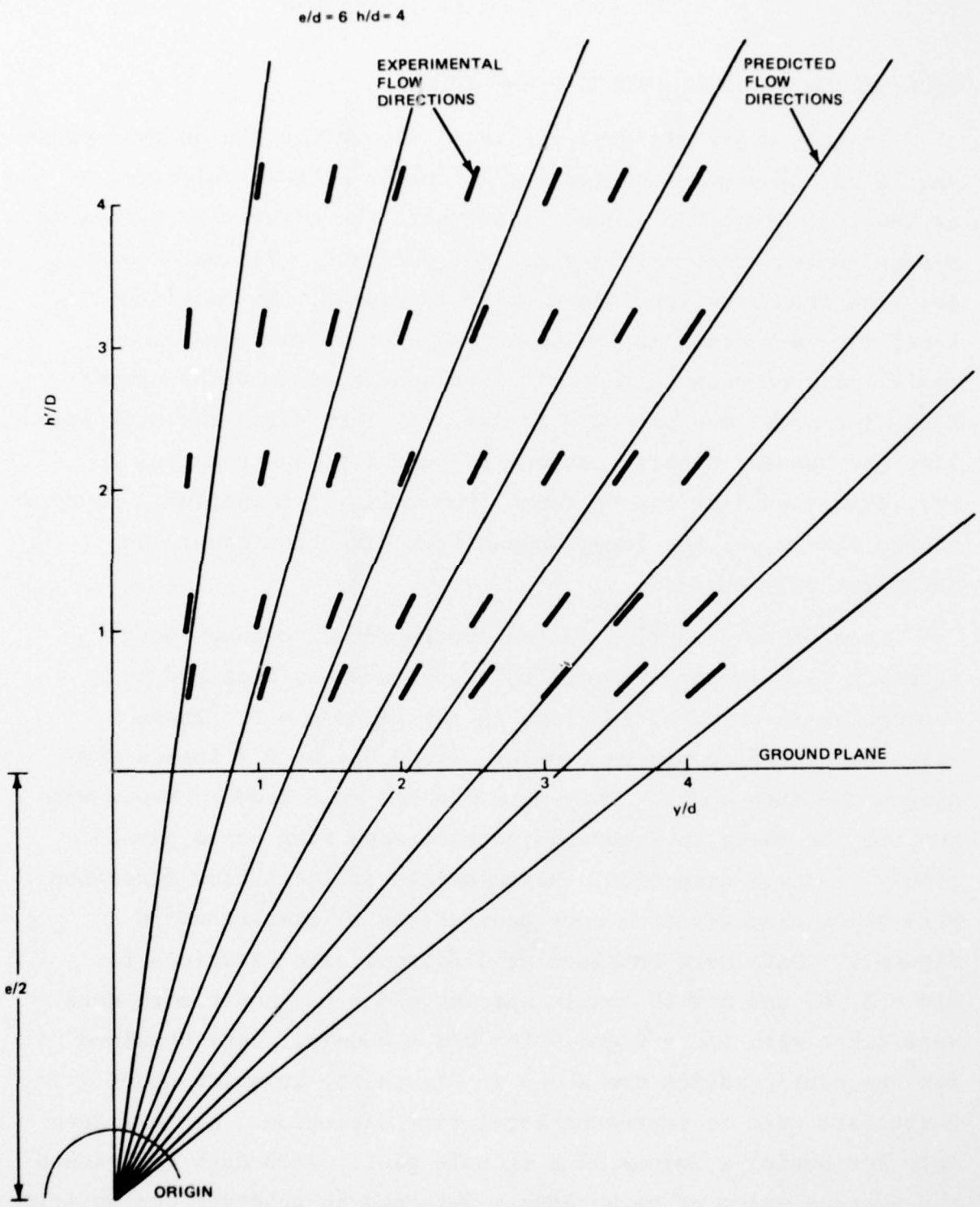
31

Fig. 16 Comparison of Measured and Predicted Upwash Flow Direction

32

values of z at the same axial station. This method of
presentation was chosen to minimize a slight lack of symmetry.
The solid lines in Figure 16 represent local flow direction as
predicted by the radial wall jet extension model described above.

Close to the ground the local flow direction was quite close
to the predicted inclination for all values of e/d. The agreement
was not as good for data taken far from the ground plane,
particularly in regions far from the central upwash. We attribute
this discrepancy to entrainment and turbulent mixing of ambient
air into the upwash. Independent measurements of local flow
inclination obtained with hot film probes, described further in
Appendix B, verified the data obtained with the flag array.

While the flow direction in the upwash appears to be radial,
the maximum upwash velocity u_o was found to decay more rapidly
than predicted by Eq. (2) for a radial wall jet. This result
may be caused by greater exposure of the upwash to mixing and
entrainment. Pitot pressure measurements were taken in the
upwash formed by two equal strength jets to determine the
upwash decay rate. Figure 17 shows pitot pressure profiles
above the ground along lines parallel to the ground pressure
survey shown in Figure 8. The maximum pressure points are
correlated with a velocity decay rate given by

$$\frac{u_o}{u_j} \sim \left(\frac{e/2+h'}{d}\right)^{-1.6} \tag{14}$$

where $(e/2 + h')$ represents the radial distance along the wall
jet and into the upwash to a point in its center h' above the
ground.

The proportionality constant in Eq. (14) can be evaluated
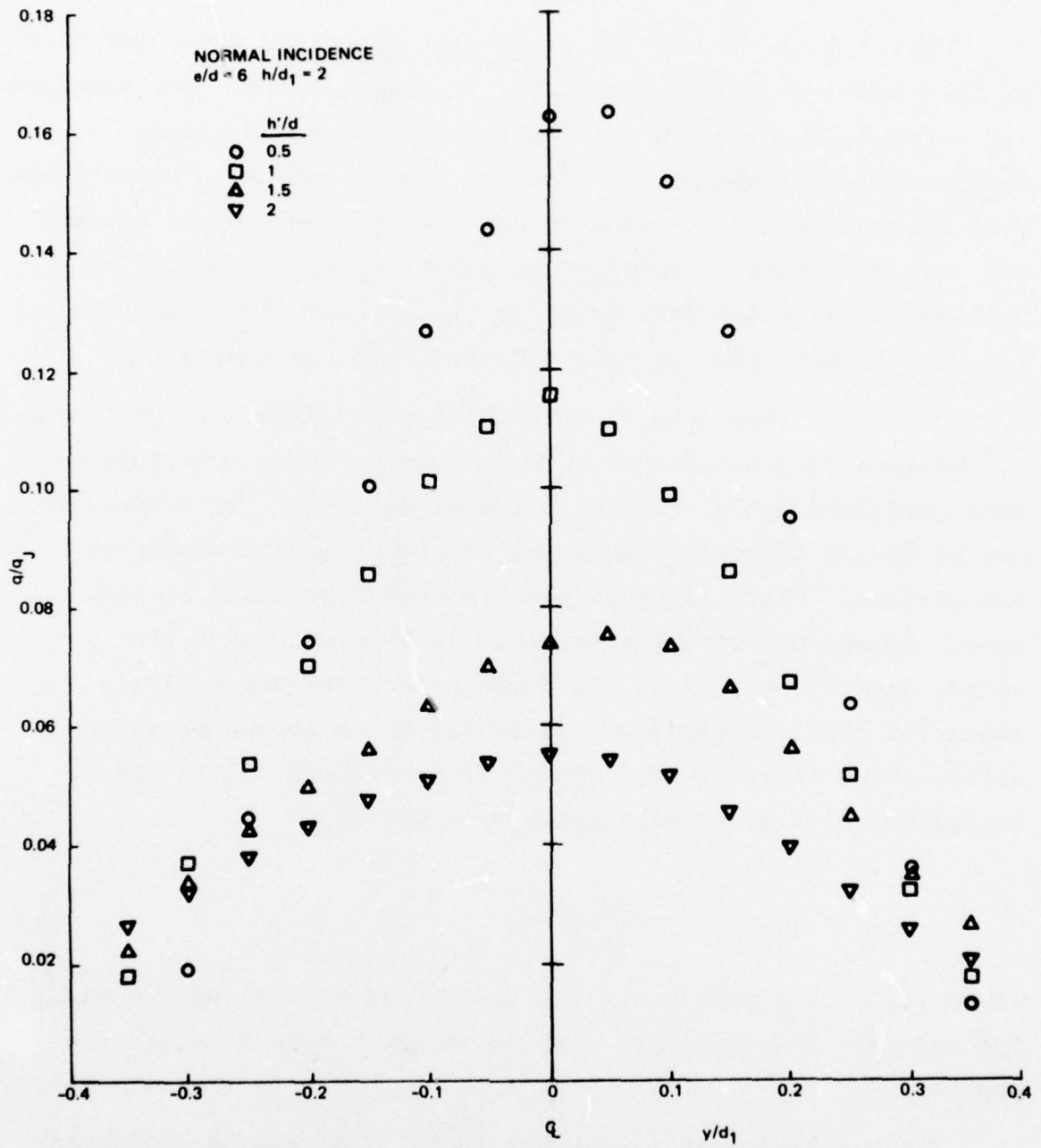from the ground surface pressure measurement in the center of

33

Fig. 17 Upwash Pitot Pressure Profiles for Equal Strength Jets

the upwash. We assume that the maximum velocity in the wall
jet is equal to u_r at the surface, which is denoted u_{ro} at
the center of the upwash. Then from Eq. (1)

$$\frac{u_{ro}}{u_j} = \sqrt{\frac{P_s - P_A}{q_j}}$$

Since the distance from the jet impact points to the stagnation
centerline is $e/2$

$$\frac{u_o}{u_j} = \sqrt{\frac{P_s - P_A}{q_j}} \left(\frac{e/2 + h'}{e/2}\right)^{-1.6} \tag{15}$$

Probe measurements were taken along the centerline of the
upwash for a range of jet exit velocities. The data are shown in
Figure 18 to illustrate correlation with the upwash velocity
decay predicted by Eq. (15). The curve shown in Figure 18 was
developed by assuming that the origin of the upwash was located
a quarter of a jet diameter above ground, which corresponds to
the wall jet half-velocity thickness at that point. The dispersion
in data for different u_j close to the ground plane occurred
because the probe was moving into the formative region of the upwash,
which is extremely narrow and not spatially stable.

The surface value of maximum upwash velocity u_r along the
entire stagnation line can be found by assuming that it is equal
to the local value of incident wall jet velocity, which is the
assumption used to evaluate the constant in Eq. (15). For normal
incidence of equal strength jets, the radial decay rate in Eq. (2)
provides the following variation of u_r with z

$$\frac{u_r}{u_{ro}} = \left[\frac{1}{\sqrt{1 + \left(\frac{2z}{e}\right)^2}}\right]^{1.1} \tag{16}$$

35
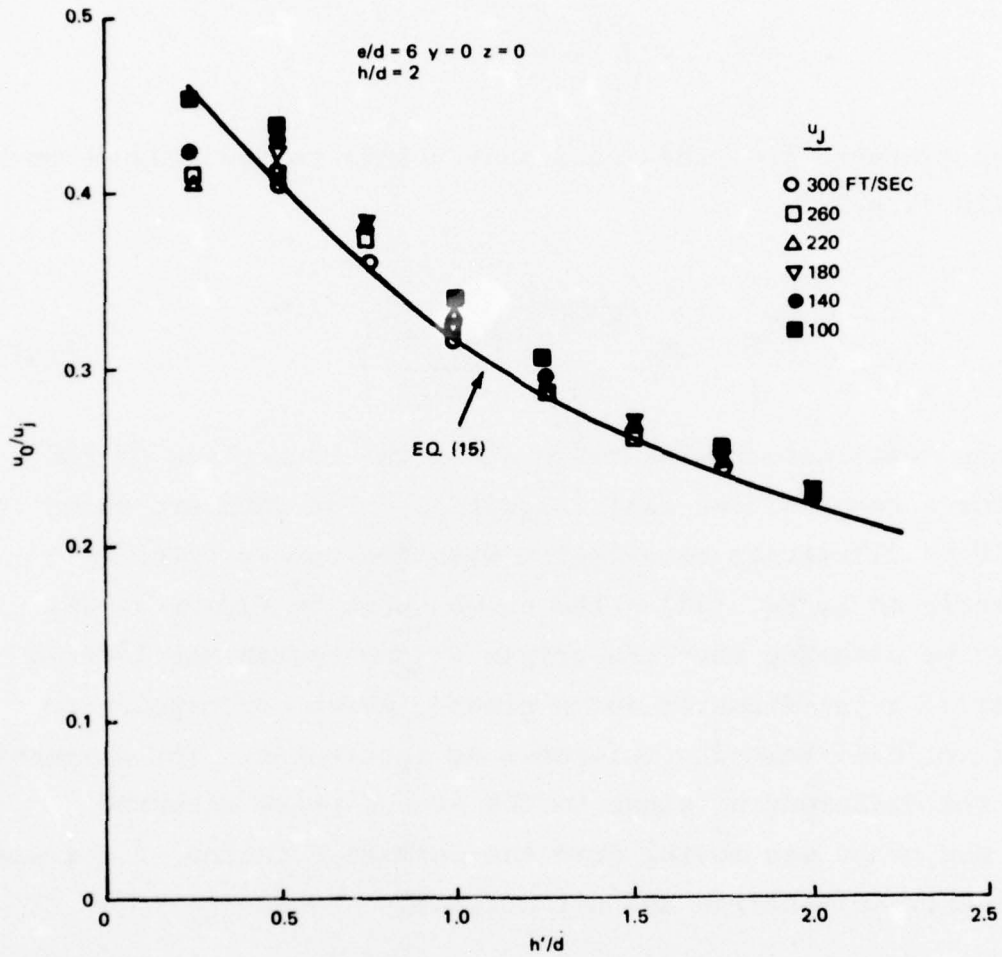
Fig. 18 Velocity Profile Along Upwash Centerline for h/d = 2

If the radial velocity decay above the ground in all regions of the upwash follows the same exponential behavior as given by Eq. (14) for u_o, then at a given height above the ground h' the upwash velocity can be found from

$$\frac{u}{u_o} = \left[\frac{1}{\sqrt{1 + \left(\frac{z}{e/2+h'}\right)^2}} \right]^{1.1} \qquad (17)$$

Figure 19 shows measurements that were taken in the upwash for comparison with pitot pressure profiles predicted by Eq. (17). These data were obtained by traversing a Keil probe at two heights above ground, with the probe aligned to the expected local flow direction at each point.

UPWASH INCLINATION FOR UNEQUAL STRENGTH JETS

The upwash inclination at the ground surface can be found by applying conservation of momentum to the two wall jets at the stagnation line. Because the velocities of the two wall jets are equal at this point, the momentum ratio m_1/m_2 is given by

$$\frac{m_1}{m_2} = \frac{\tau_1}{\tau_2}$$

where τ is the wall jet thickness. Following Glauert's wall jet model with $\tau \sim r$, we find that since the growth rates of both wall jets should be equal

$$\frac{\tau_1}{\tau_2} = \frac{y_1'}{y_2'} \qquad (18)$$

Then the upwash angle θ relative to a line normal to the surface is

37
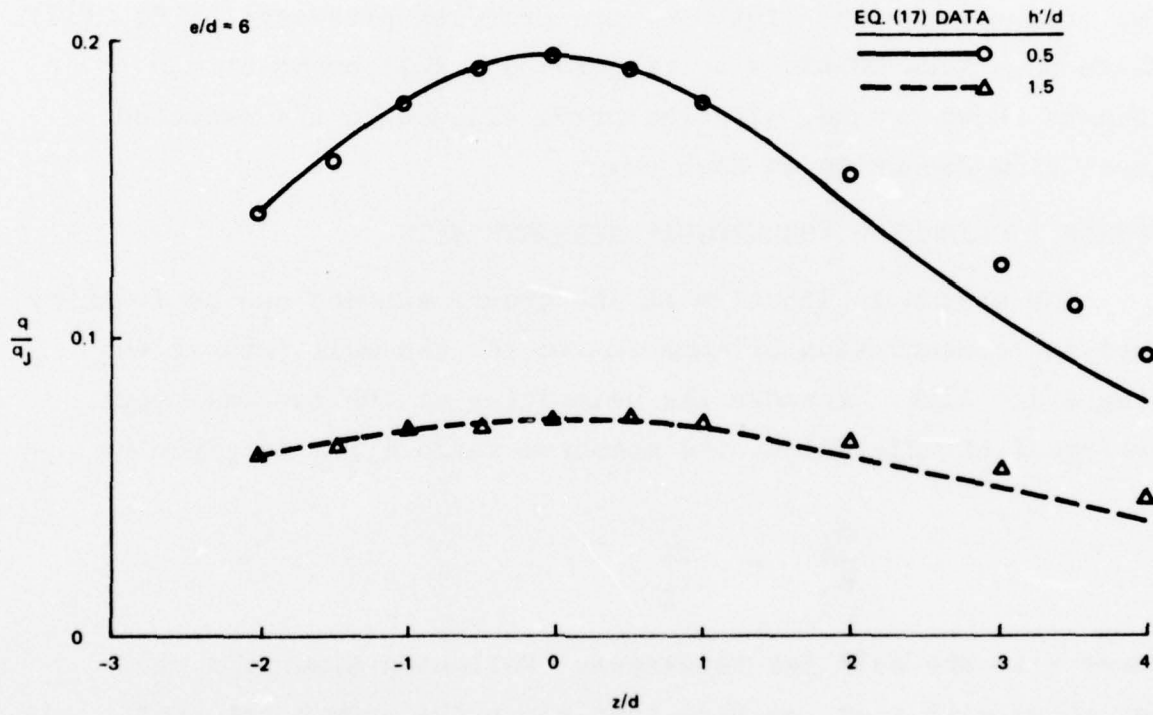
Fig. 19 Pitot Pressure Profiles Along Upwash for h/d = 3

$$\theta = \sin^{-1}\left(\frac{m_1 - m_2}{m_1 + m_2}\right) = \sin^{-1}\left(\frac{y_1/y_2 - 1}{y_1/y_2 + 1}\right) \tag{19a}$$

and from Eq. (4)

$$\theta = \sin^{-1}\left(\frac{d_{j1}/d_{j2} - 1}{d_{j1}/d_{j2} + 1}\right) \tag{19b}$$

Comparison of Eq. (5) and Eq. (19b) shows

$$\theta = \sin^{-1}\left(\frac{y_o}{e/2}\right) \tag{20}$$

An interesting conclusion from Eq. (20) is that the upwash inclination angle can be determined directly from measurement of the displacement of the stagnation line.

Pitot probe measurements were taken in the upwash formed between jets of unequal strength to determine the upwash inclination. Probe traverses were taken in the plane z = 0 parallel to the ground plane, and upwash direction was deduced from relative displacements of the maximum pressure points in profiles taken at different distances above the ground. These profiles are presented in Appendix A. In Figure 20 we have plotted the z-coordinate of the maximum point in each profile versus distance from the ground. This figure shows the variation of upwash location and inclination angle with jet strength ratio. The filled symbols represent the stagnation line location as determined by surface oil flow studies. Note that for each nozzle configuration the oil flow line location is offset from the point one would obtain by extrapolating to the ground plane a fit to the maximum points in the pressure profiles. This offset reflects the fact that the formation of the upwash occupies a considerable thickness above the ground where the wall jets collide. In this region

39

NORMAL INCIDENCE
$e/d = 6$ $h/d_1 = 2$

d_2/d_1
○ 0.81
□ 0.75
△ 0.515
▽ 0.405
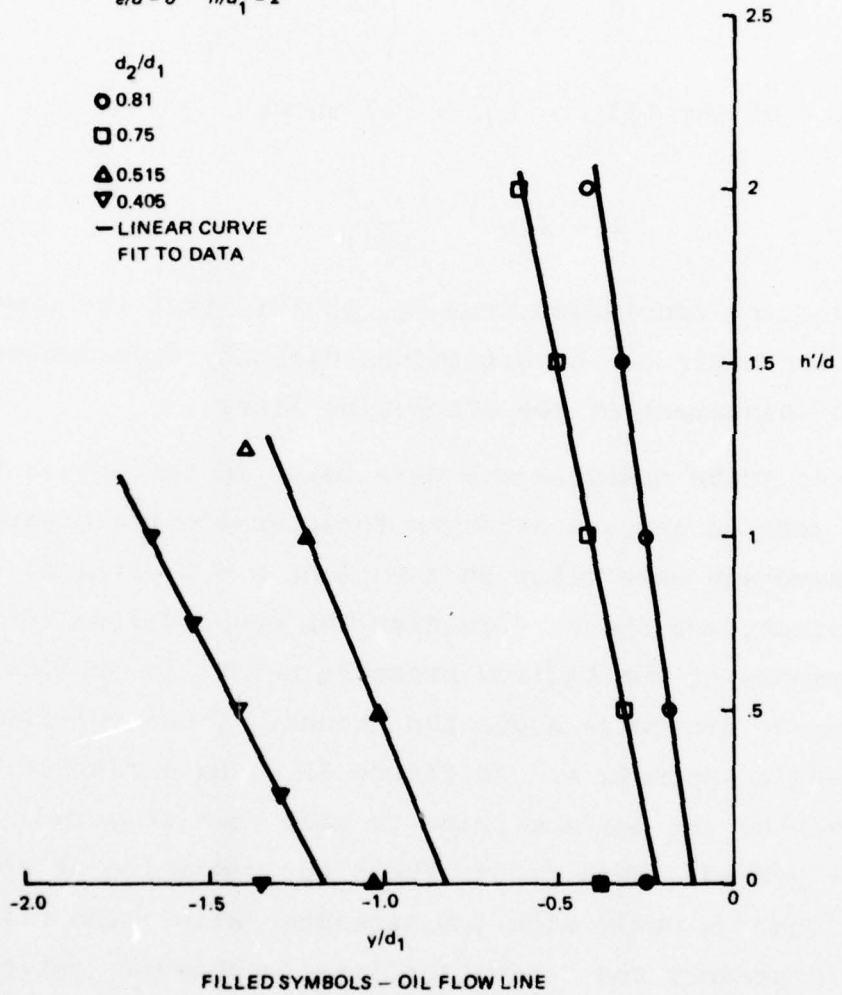— LINEAR CURVE
FIT TO DATA

FILLED SYMBOLS — OIL FLOW LINE

Fig. 20 Upwash Inclination for Unequal Strength Jets

40

the upwash flow properties undergo strong spatial gradients
that cause a local curvature of the upwash just above the ground
plane. We believe that an appropriate boundary condition is that
the streamline direction at the stagnation point is normal to
the ground.

Figure 21 shows the variation of upwash inclination angle
with jet diameter ratio predicted by Eq. (19b) compared to
inclination angles measured from Figure 20. Also shown in
Figure 21 are values of θ that were deduced from measured oil
line displacements using Eq. (20).

UPWASH INCLINATION FOR INCLINED JETS

Again, applying conservation of momentum to the wall jets
at the stagnation line, where the maximum velocities should be
equal, we find the wall jet momentum ratio equal to the local
thickness ratio. Donaldson and Snedeker (Ref. 7) found for a
single jet impinging at an angle σ_J that the wall jet growth
rate was independent of ϕ. If the wall jet growth rate is also
independent of h/d, then we can apply Eq. (19a) to this case
also, using the distances between the upwash line and the displaced
stagnation points for y_1 and y_2.

Pitot probe measurements were taken in the upwash formed
between equal strength jets impinging at different angles σ_J.
Pitot pressure profiles taken at different heights above the
ground are presented in Appendix A. In Figure 22 we have
plotted the z-coordinate of the maximum point in each profile
versus distance from the ground. Taking measurements of y_1 and
y_2 from the ground plane pressure measurements presented in
Appendix A, Eq. (19a) predicts $\theta = 9^o$, 19°, and 34° for $\sigma_J =$
80°, 70°, and 60°. Our data shows lower values of upwash
inclination. In addition, the data in Figure 22 shows that the

41
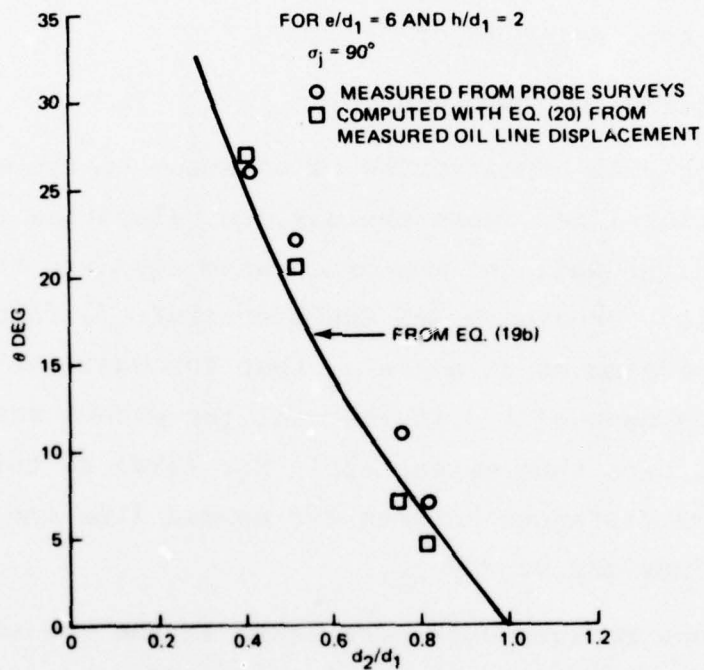
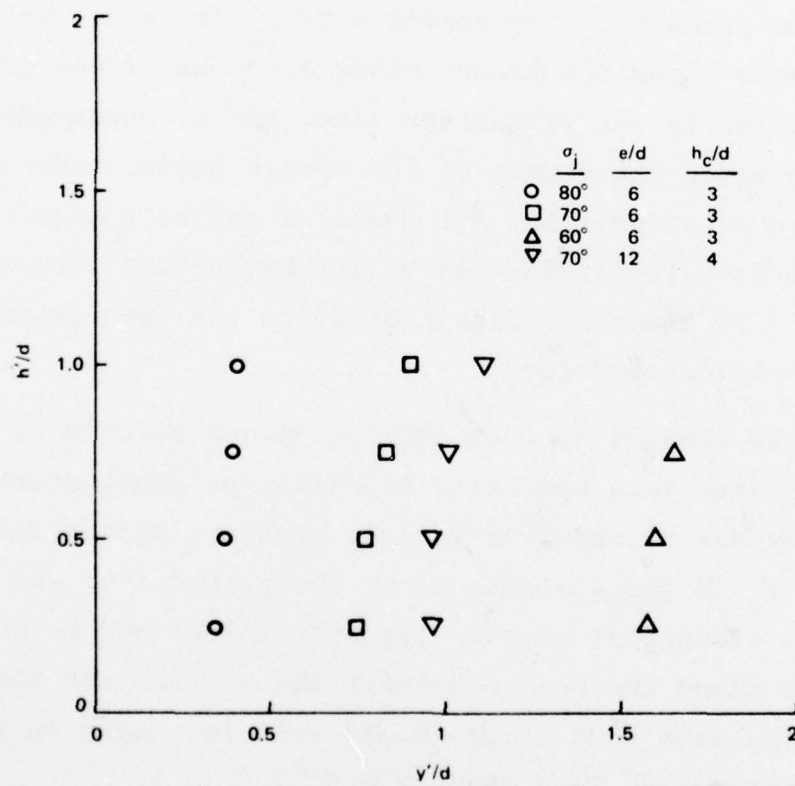Fig. 21 Effect of Jet Strength Ratio on Upwash Inclination

Fig. 22 Upwash Inclination for Inclined Jets

43

upwash path between inclined jets appears to be curved, with the upwash angle θ increasing with distance above the ground.

VELOCITY DECAY IN DISPLACED UPWASH

When the upwash is displaced from the midpoint between jet impact points, either because of unequal jet strength or because of jet inclination, the maximum velocity along the upwash center-line was found to decay more rapidly than predicted by Eq. (15). Figure 23 shows a plot of maximum velocities taken from field surveys obtained using jets of unequal strength. Velocities have been normalized by u_r as determined from measured central upwash ground pressure. The abscissa is $r_s/(r_s + h'')$ where r_s is the distance along the ground plane from the impact point of the stronger jet to the stagnation line, and h'' represents the distance along the center of the upwash between the surface and the probe location. For jet diameter ratios between 0.75 and 1.0, the data falls close to a line having the same slope as Eq. (15). At lower jet diameter ratios the data exhibits a more rapid velocity decay.

Figure 24 shows a plot of maximum upwash velocities produced by equal strength jets operating at different impingement angles. Again, u_r was determined from surface pressure measurement. For this figure r_s is the distance along the ground from the impact point of the closer jet to the stagnation line, and h'' represents the distance along the upwash between the surface and the probe location. The data show a more rapid velocity decay in the upwash at impingement angles less than $\sigma_J = 90°$.

Figures 23 and 24 bring out a basic problem in our modeling of the upwash flow field. If the jet impingement angle is close to normal, or if the jet strength ratio is close to 1, the upwash can be visualized (approximately) as a continuation of

44
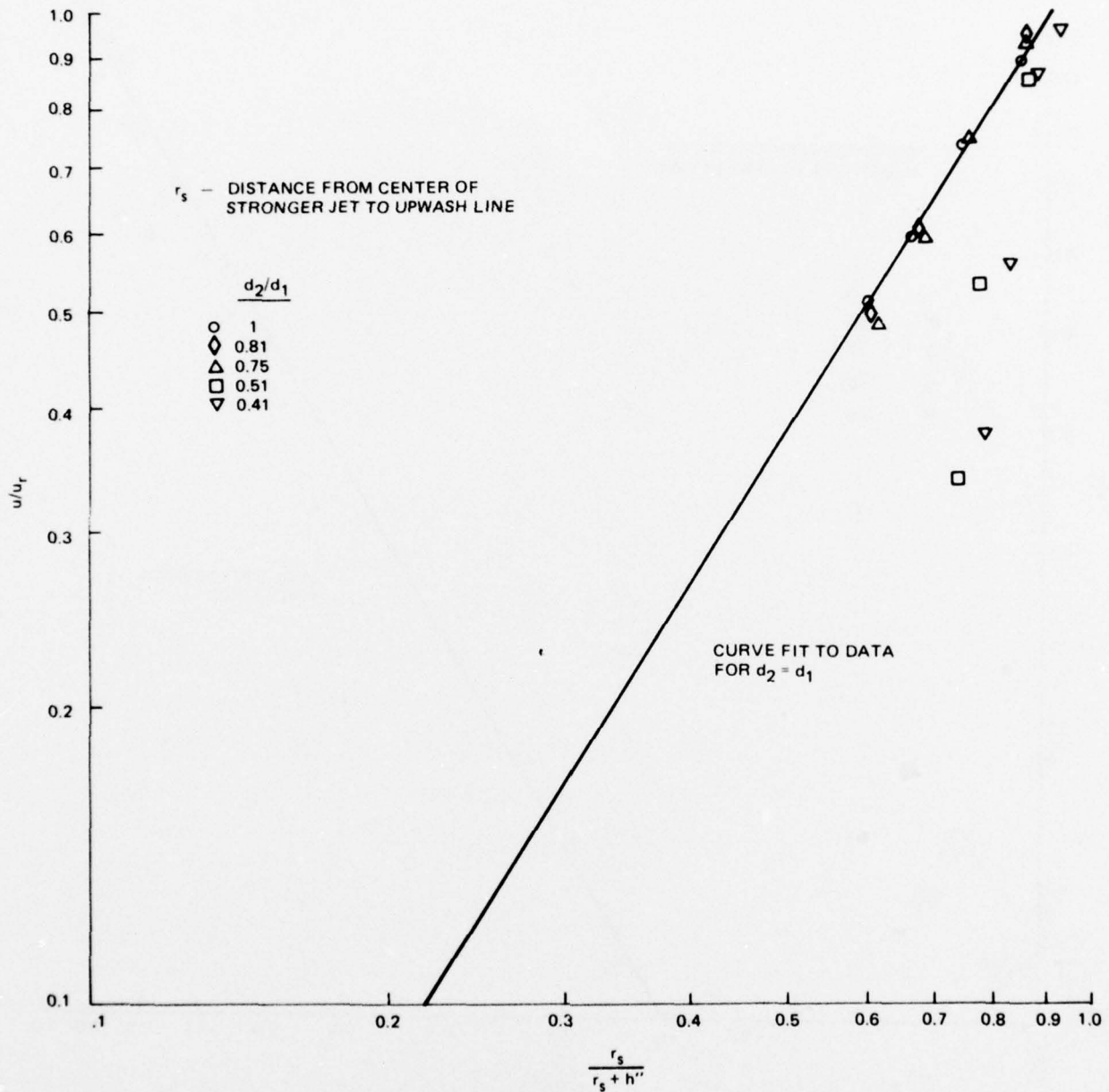
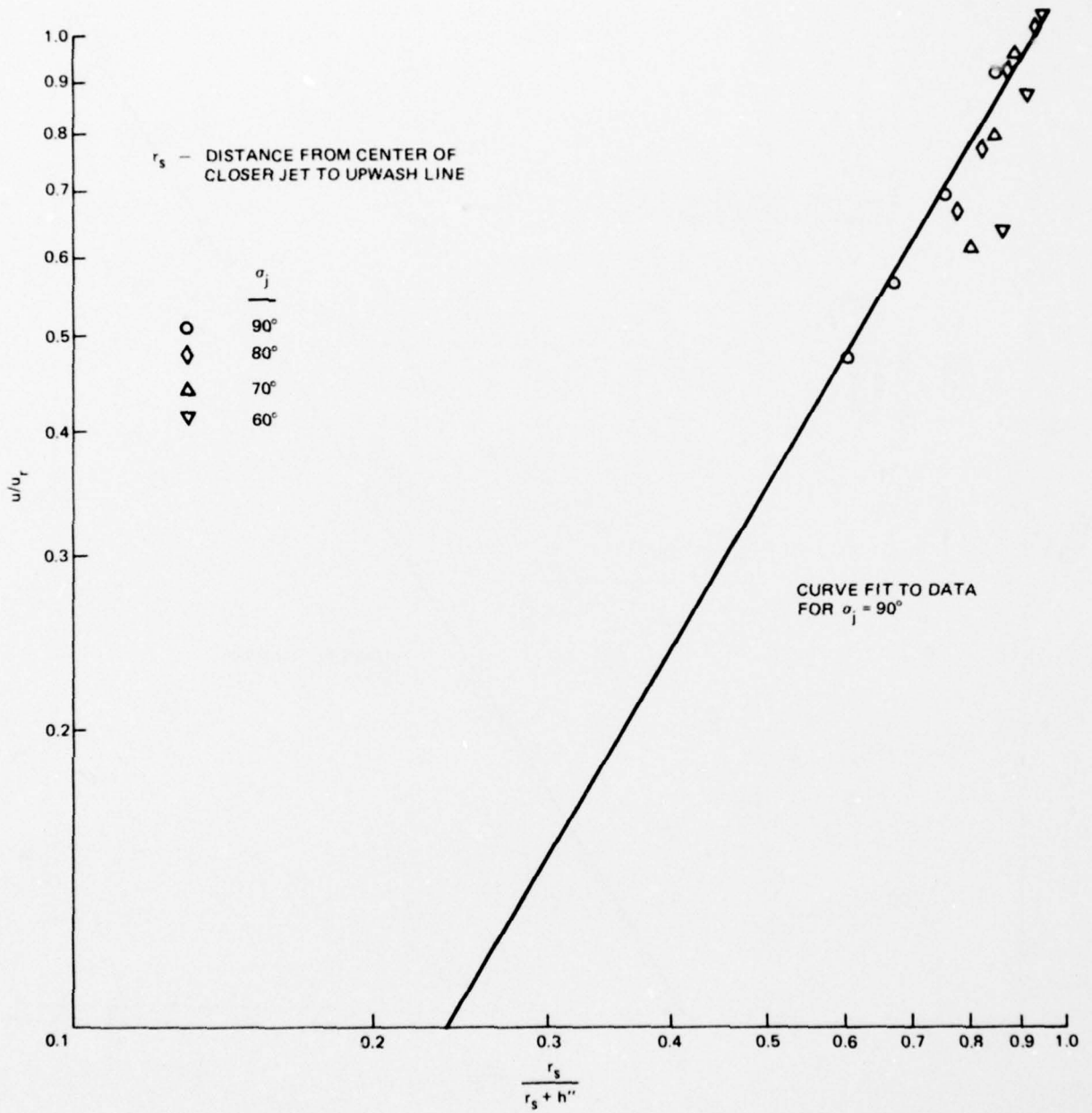Fig. 23 Effect of Jet Strength Ratio on Upwash Velocity Decay

Fig. 24 Effect of Jet Impingement Angle on Upwash Velocity Decay

46

radial flow from colliding wall jets, with the decrease in
upwash velocity above the surface exhibiting a power law
dependence on radius. However, when nonsymmetric impingement
conditions produce a large displacement of the stagnation
line from the midpoint between jet impact points, this radial
flow model for the upwash should breakdown. If the stagnation
line is closer to one jet impact point, the local wall jet
divergence angles approaching the stagnation line are different
on both sides. Under such conditions the deflection of the
two wall jet flows away from the ground surface would yield
local flow inclination angles (within the plane of the upwash)
that were unequal. The mixing of two directionally misaligned
flows may lead to greater mixing and entrainment of ambient
air, which would provide a more rapid maximum velocity decay
along the upwash centerline.

5. CONCLUSIONS

For two equal strength jets impinging normal to the ground, the local flow direction in the upwash agreed with predictions of a model that assumed radial flow from the jet impingement points to the stagnation line, followed by continued radial flow into the upwash. The measured maximum centerline upwash velocity above the ground plane agreed with values predicted from surface pressure data. The centerline upwash velocity was relatively independent of ground plane distance, and its variation with nozzle separation distance was scaled in accordance with known wall jet behavior. The centerline velocity in the upwash followed a power law decay above the ground. The rate of decay was more rapid than that encountered in a wall jet and appeared to be independent of incident jet velocity. Prediction of the transverse velocity variation along the upwash that were based on an existing wall jet model showed close agreement with data.

For unsymmetric impingement conditions, developed by either unequal strength jets or by ground plane inclination, the upwash was displaced from the midpoint between jet impact points. Approximate analyses were developed to predict the curvature of the ground stagnation line in terms of jet strength ratio or jet impingement angle. For normal ground impingement of jets of unequal strength, the upwash displacement and inclination were found to be predictable in terms of jet strength ratio. For equal strength jets impinging on an inclined ground, the upwash displacement could be predicted in terms of jet impingement angle, but its inclination could not. The path of the upwash between inclined incident jets was found to be curved, leaving the surface at clost to 90° for all jet inclination angles.

49

Agreement between measured and predicted upwash behavior
was closer for variation of jet strength ratio than for variation
of jet impingement angle. Modeling of the upwash formed by two
inclined incident jets was based on existing wall jet data
obtained from impingement tests with a single inclined jet. More
accurate predictions could be made if sufficient data were
available to define the variation of wall jet properties with
ground separation distance for a single inclined jet.

Local flow measurements were made in the upwash flows with
pitot probes and with hot film anemometers. Strong fluctuations
in flow properties were found throughout the upwash, and the
magnitude of these fluctuations increased with jet height above
the ground. Because of the almost unsteady nature of the upwash
we found that local mean flow properties generally could be
measured more accurately with a pitot tube than with a hot film
anemometer.

6. REFERENCES

1. Gentry, G.L. and Margason, R.J., "Jet Induced Lift Losses on VTOL Configurations Hovering In and Out of Ground Effect," NASA TN D-3166, February 1966.

2. Skifstad, J.G., "Aerodynamics of Jets Pertinent to VTOL Aircraft," Journal of Aircraft, Vol. 7, No. 3, pp. 193-204, May-June 1970.

3. Siclari, M.J., Migdal, D., Luzzi, T.W., Jr., Barche, T., and Palcza, J.L., "Development of Theoretical Models for Jet-Induced Effects on V/STOL Aircraft," Journal of Aircraft, Vol. 13, No. 12, pp. 938-944, December 1976.

4. Hill, W.G., Jr. and Jenkins, R.C., "Experimental Investigation of Multiple Jet Impingement Flows Applicable to VTOL Aircraft in Ground Effect," Grumman Research Department Memorandum RM-605, November 1975.

5. Pankhurst, R.C. and Holder, D.W., Wind-Tunnel Technique, Sir Isaac Pitman and Sons, Ltd, 1952.

6. Glauert, M. B., "The Wall Jet," Journal of Fluid Mechanics, Vol. 1, December 1956, pp. 625-643.

7. Donaldson, C. DuP. and Snedeker, R.S., "A Study of Free Jet Impingement. Part I. Mean Properties of Free and Impinging Jets," Journal of Fluid Mechanics, Vol. 45, Part 2, pp. 281-319, 1971.

8. Gray, L. and Kisielowski, E., "Practical Engineering Methods for Predicting Hot Gas Reingestion Characteristics of V/STOL Aircraft Jet-Lift Engines," NASA-CR 111845, February 1971.

APPENDIX A

GROUND PLANE AND UPWASH FLOW FIELD DATA

Fig. A-1 Ground Pressure Distribution — Normal Impingement of Equal Strength Jets, Sheet 1 of 2

d = 2 IN.
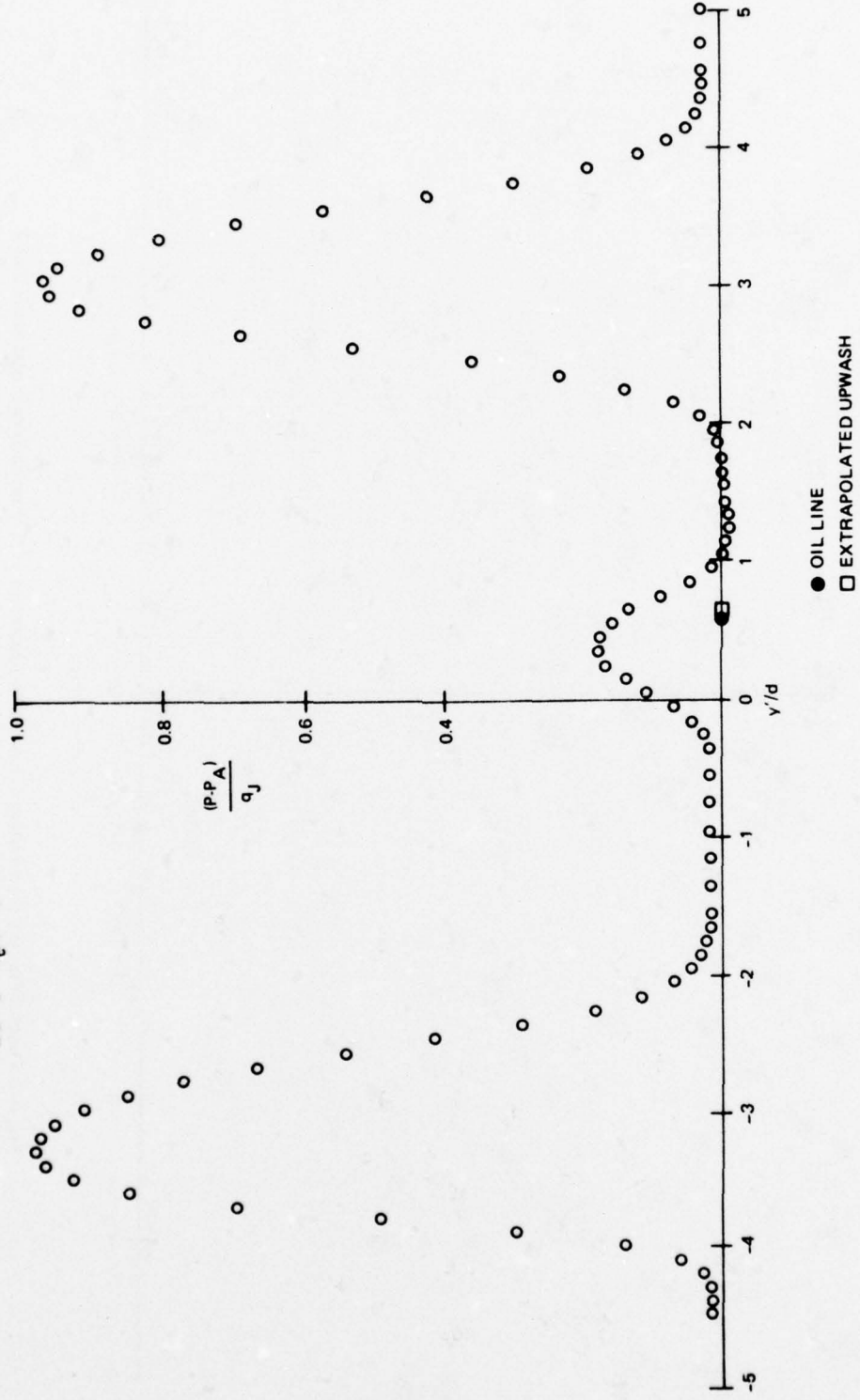e/d = 6 $h_c/d = 3$
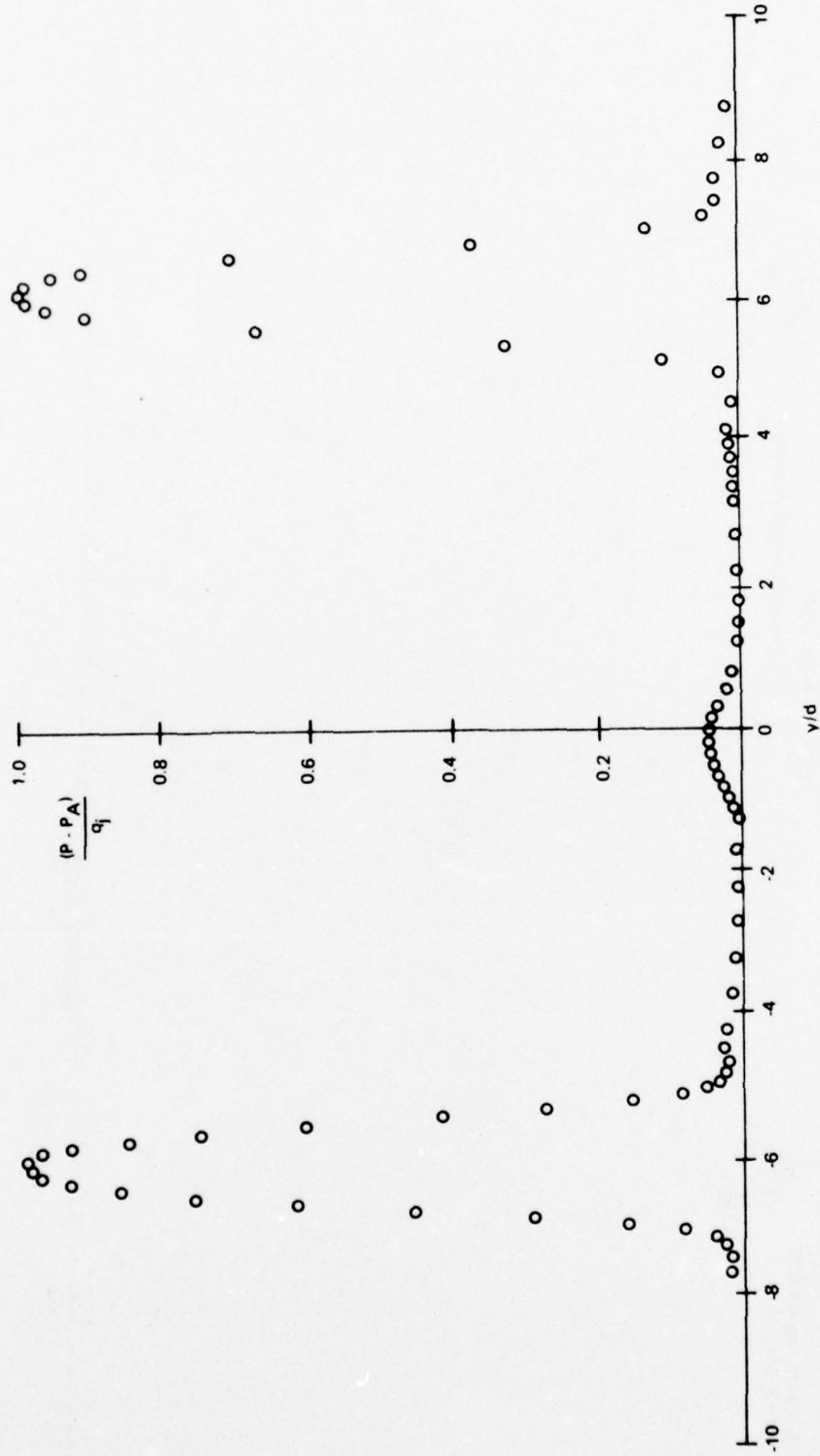
$\frac{(P - P_A)}{q_j}$

y/d

Fig. A-1 Ground Pressure Distribution – Normal Impingement of Equal Strength Jets, Sheet 2 of 2

A-3

Fig. A-2 Ground Pressure Distribution — Normal Impingement of Unequal Strength Jets Sheet 1 of 2

A-4
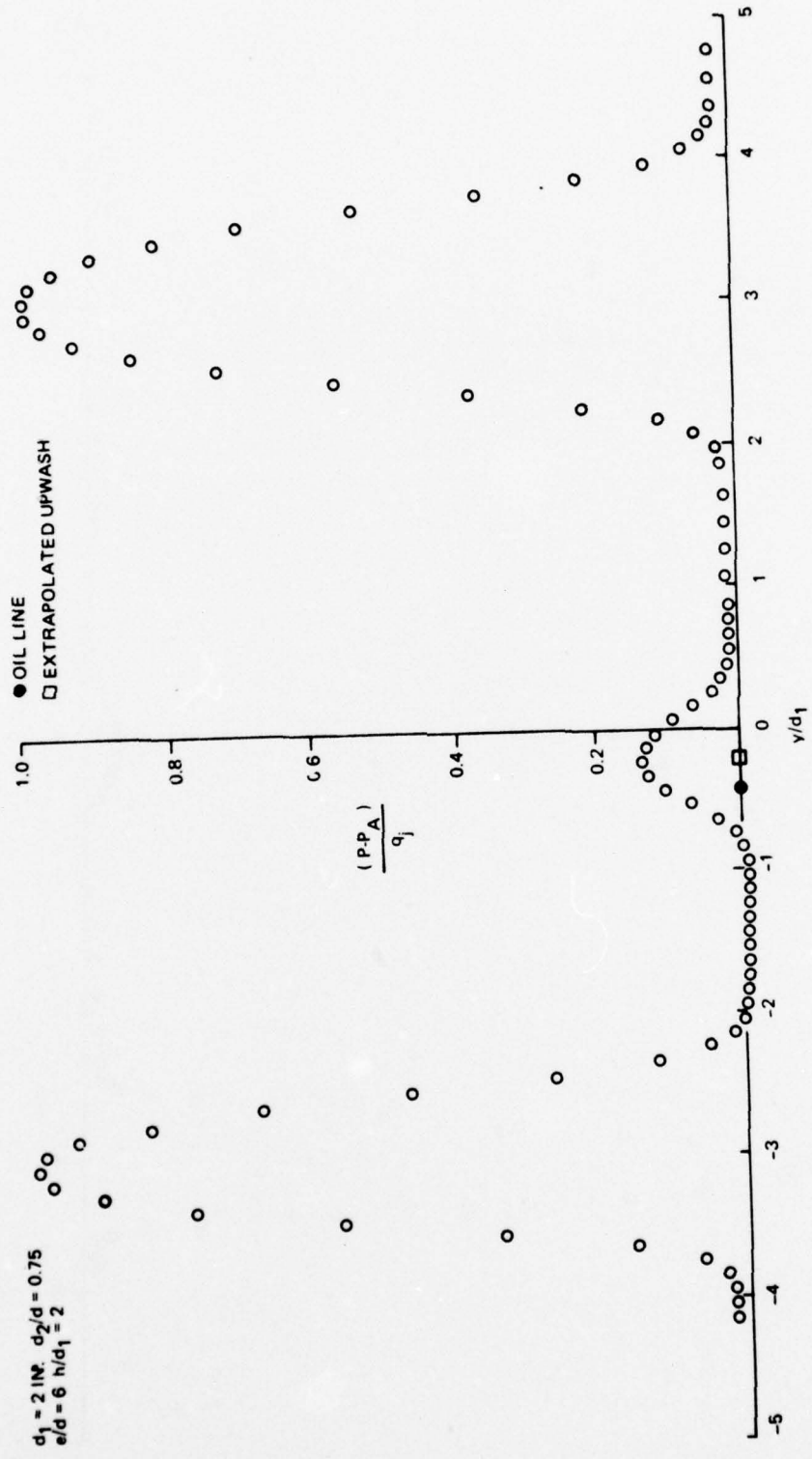
● OIL LINE
☐ EXTRAPOLATED UPWASH

$d_1 = 2$ IN. $d_2/d_1 = 0.515$
$e/d = 6$ $h/d_1 = 2$

Fig. A-2 Ground Pressure Distribution — Normal Impingement of Unequal Strength Jets Sheet 2 of 2

A-5

d = 2 IN. $\sigma_j = 80°$
e/d = 6 $h_c/d = 3$

$\dfrac{(P-P_A)}{q_J}$

y'/d

● OIL LINE
□ EXTRAPOLATED UPWASH
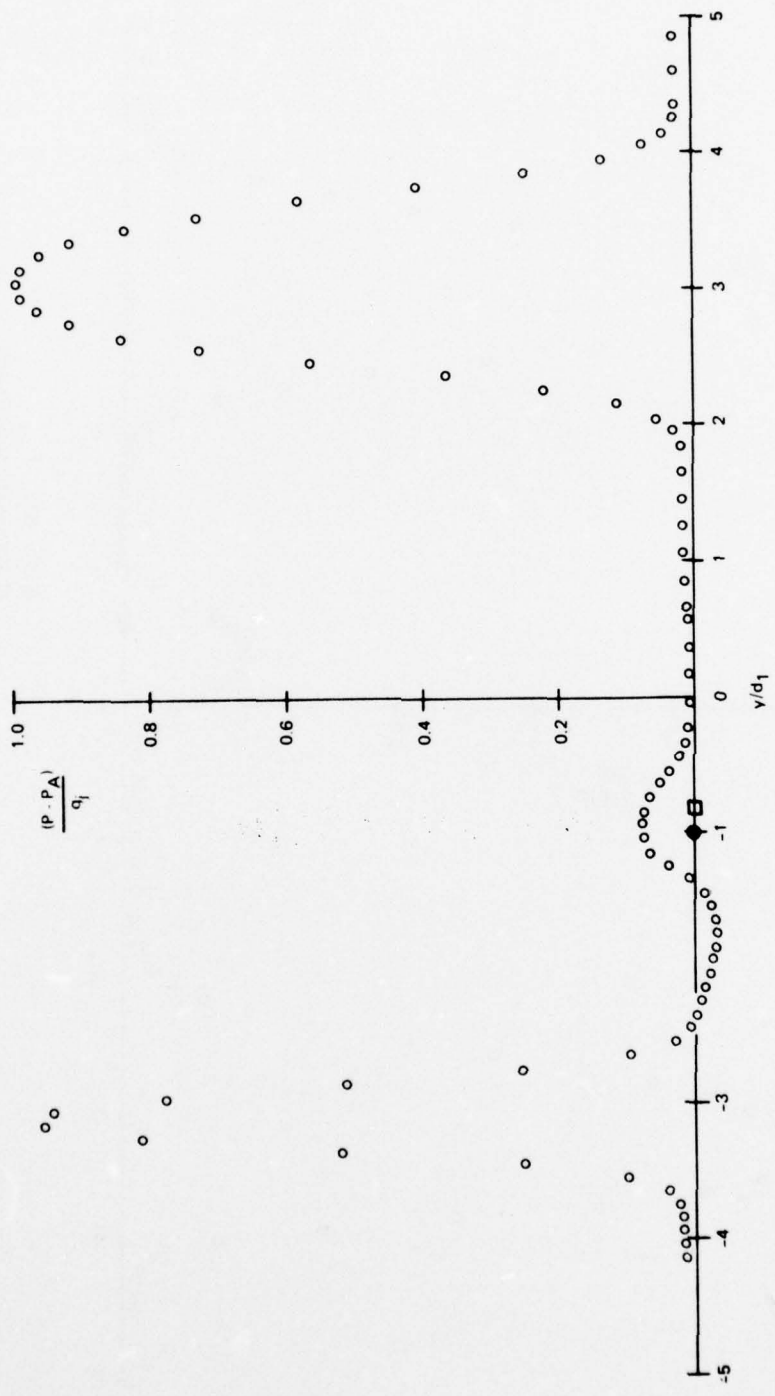
Fig. A-3 Ground Pressure Distribution — Inclined Impingement of Equal Strength Jets, Sheet 1 of 3
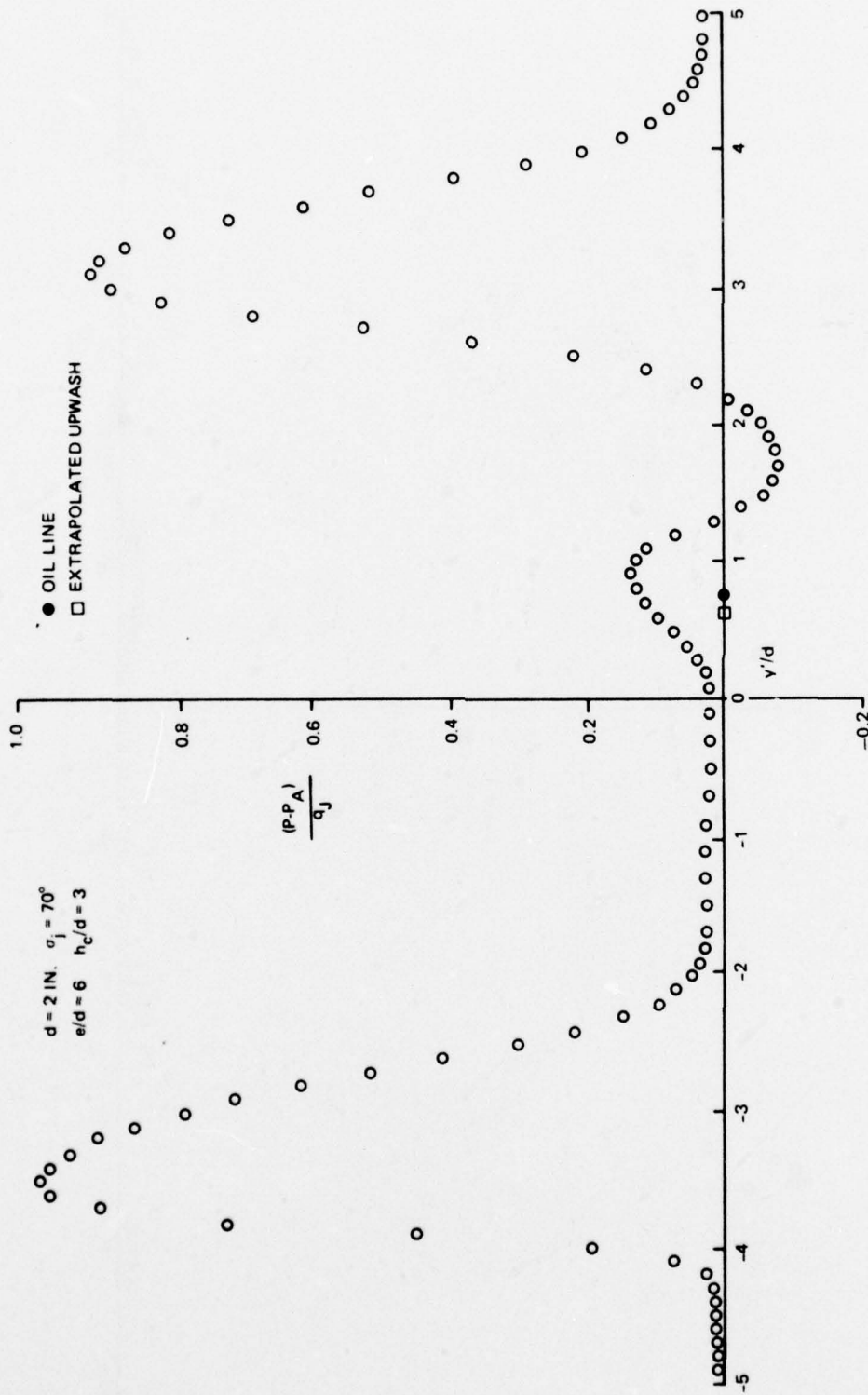
A-6

Fig. A-3 Ground Pressure Distribution — Inclined Impingement of Equal Strength Jets, Sheet 2 of 3

$d = 1$ IN. $\sigma_J = 70°$
$e/d = 12$ $h_c/d = 4$

$\dfrac{(P-P_A)}{q_J}$

y/d
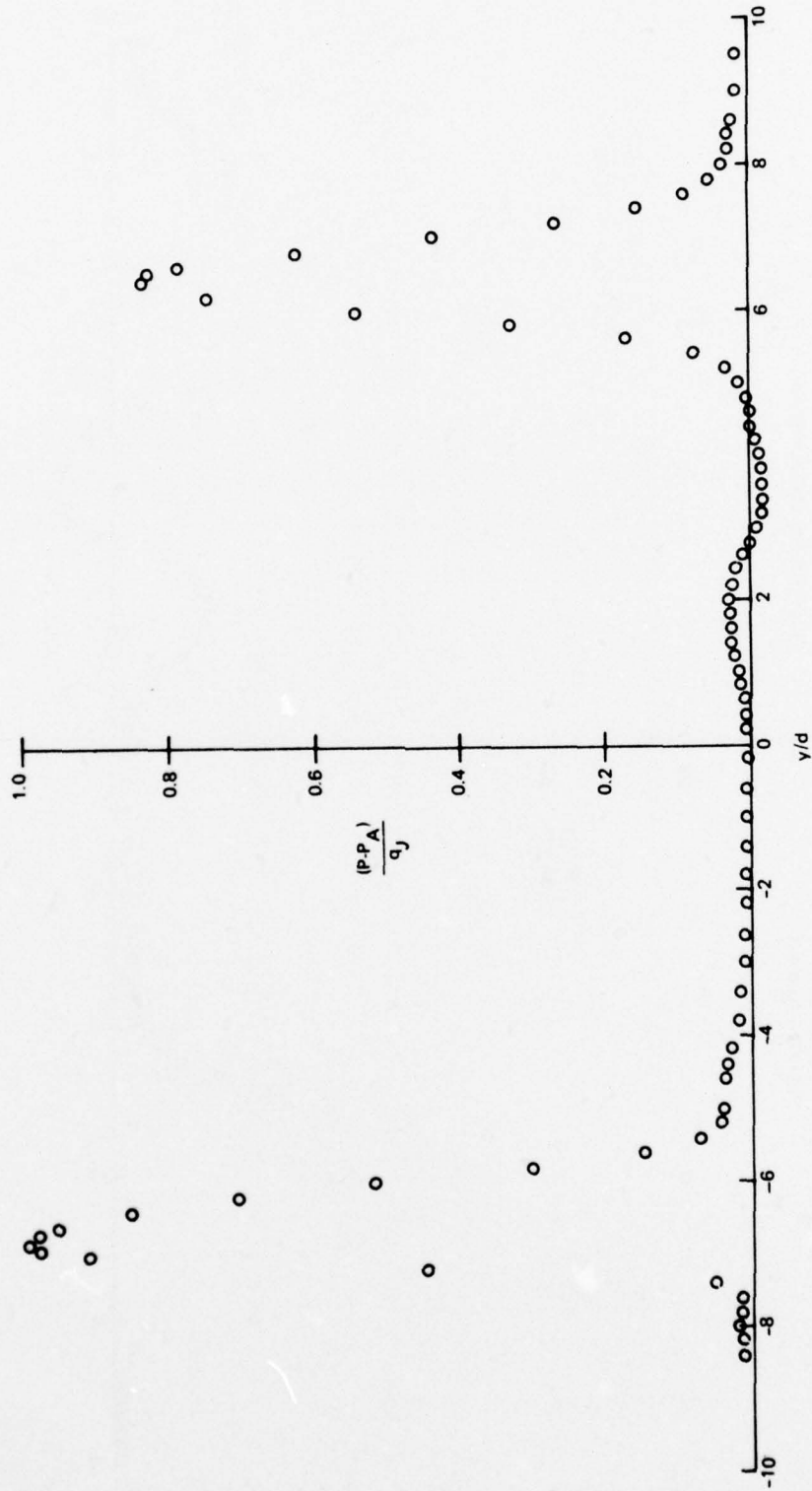
Fig. A-3 Ground Pressure Distribution – Inclined Impingement of Equal Strength Jets, Sheet 3 of 3

A-8
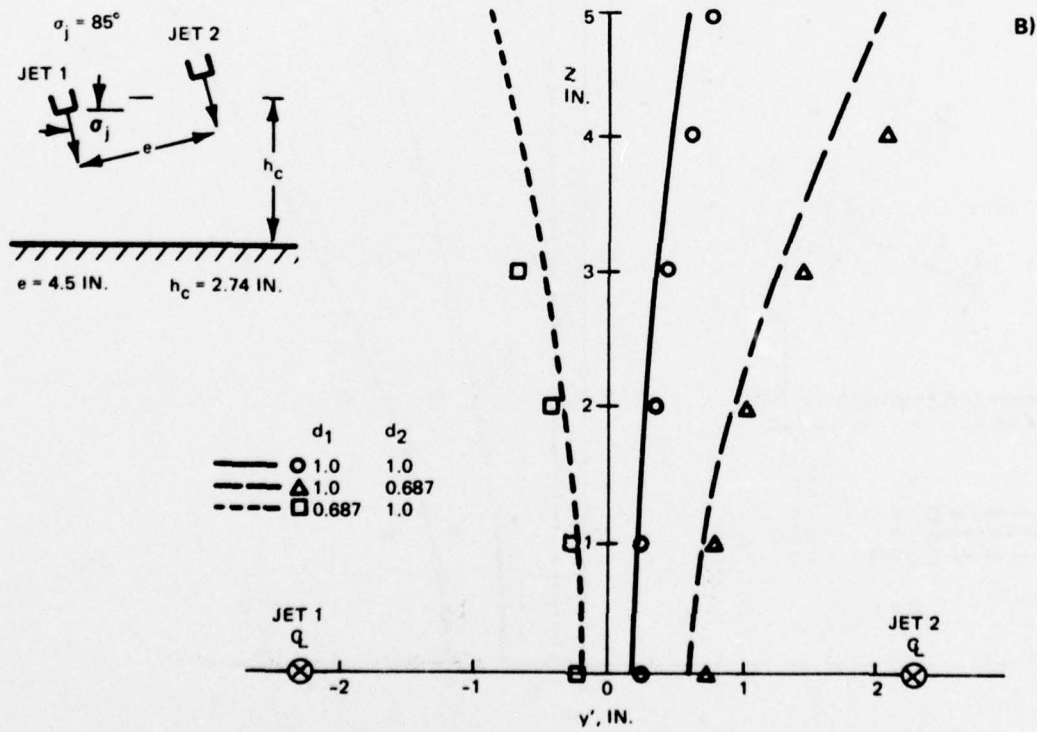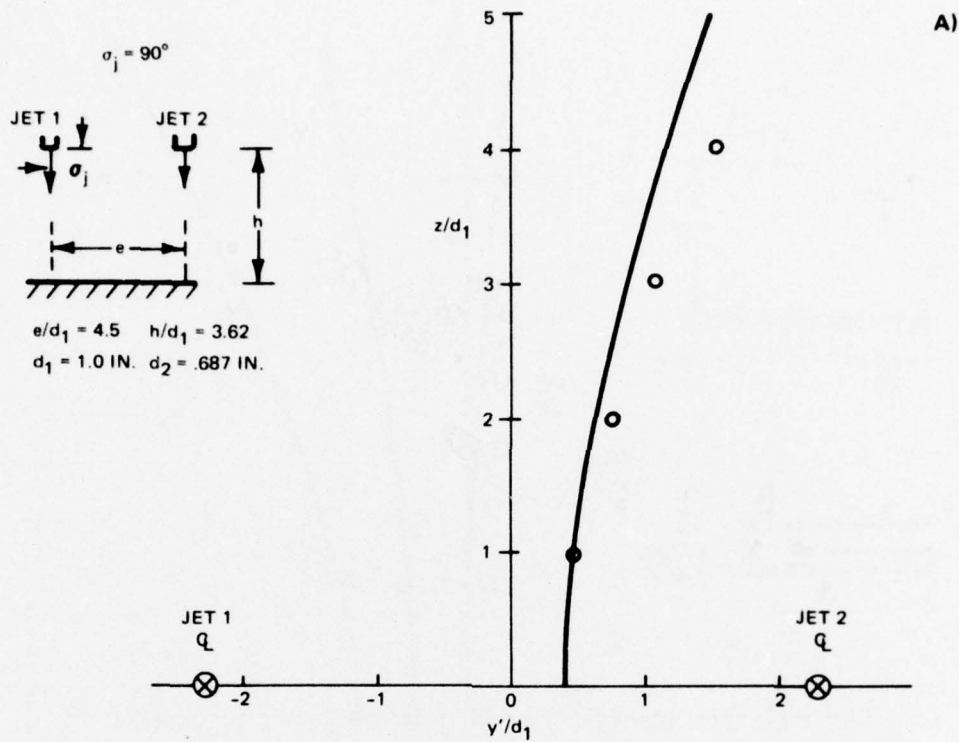
Fig. A-4 Comparison of Measured and Computed Stagnation Line Shapes, Sheet 1 of 3

A-9
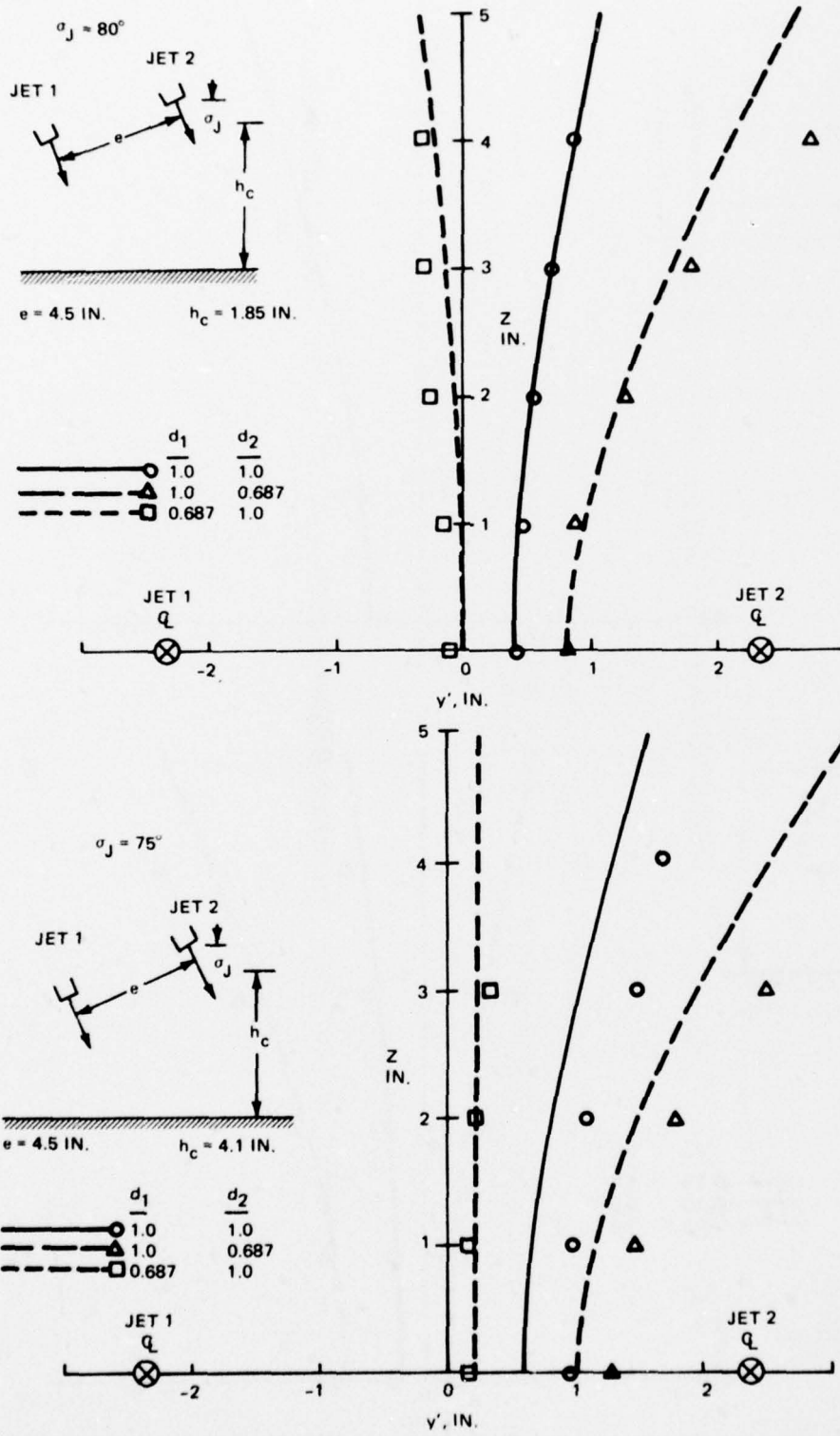
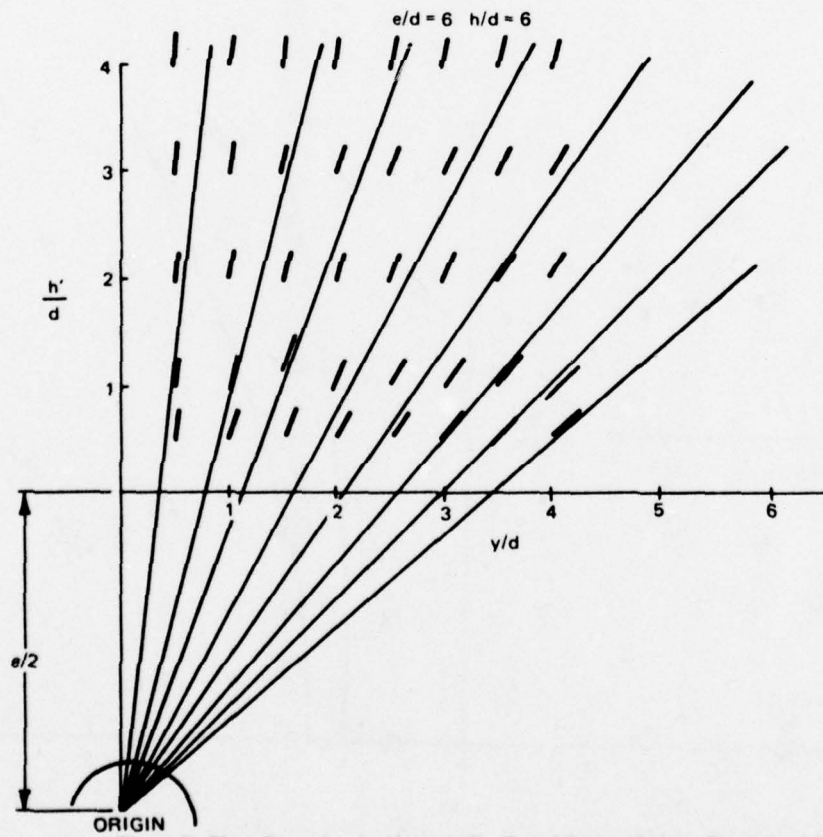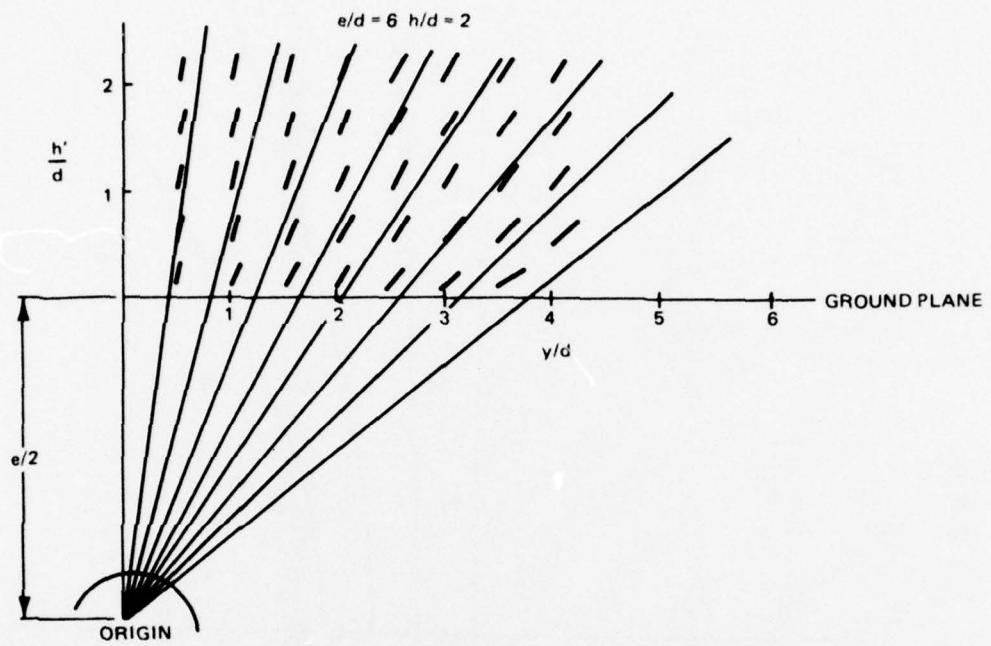Fig. A-4 Comparison of Measured and Computed Stagnation Line Shapes, Sheet 2 of 3
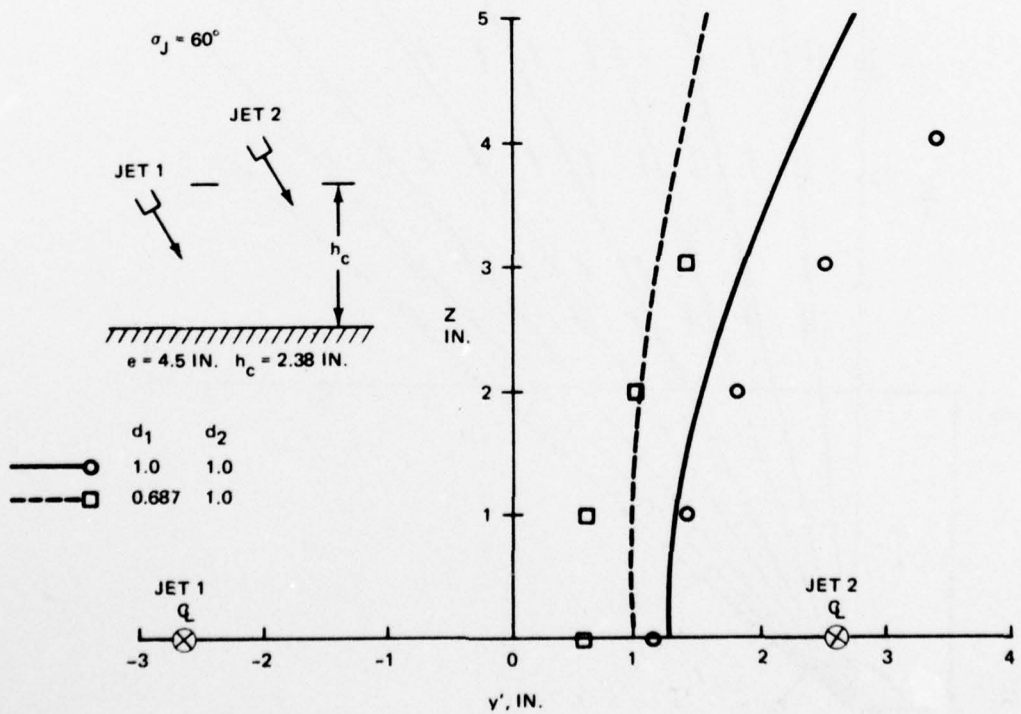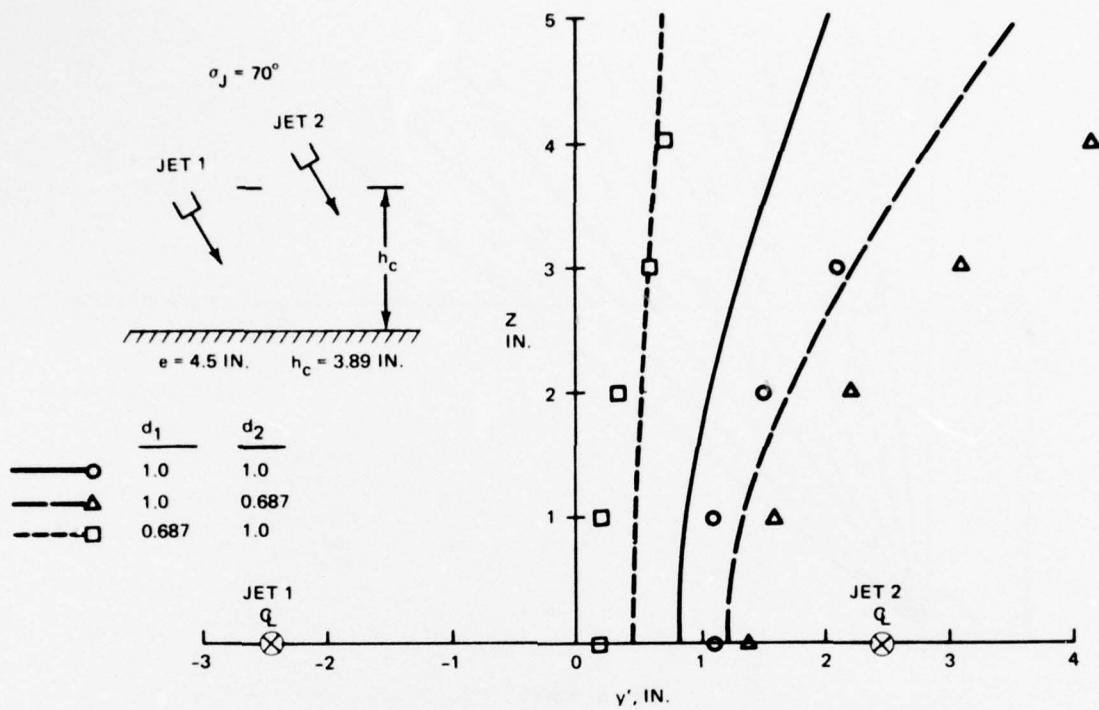
Fig. A-4 Comparison of Measured and Computed Stagnation Line Shapes, Sheet 3 of 3

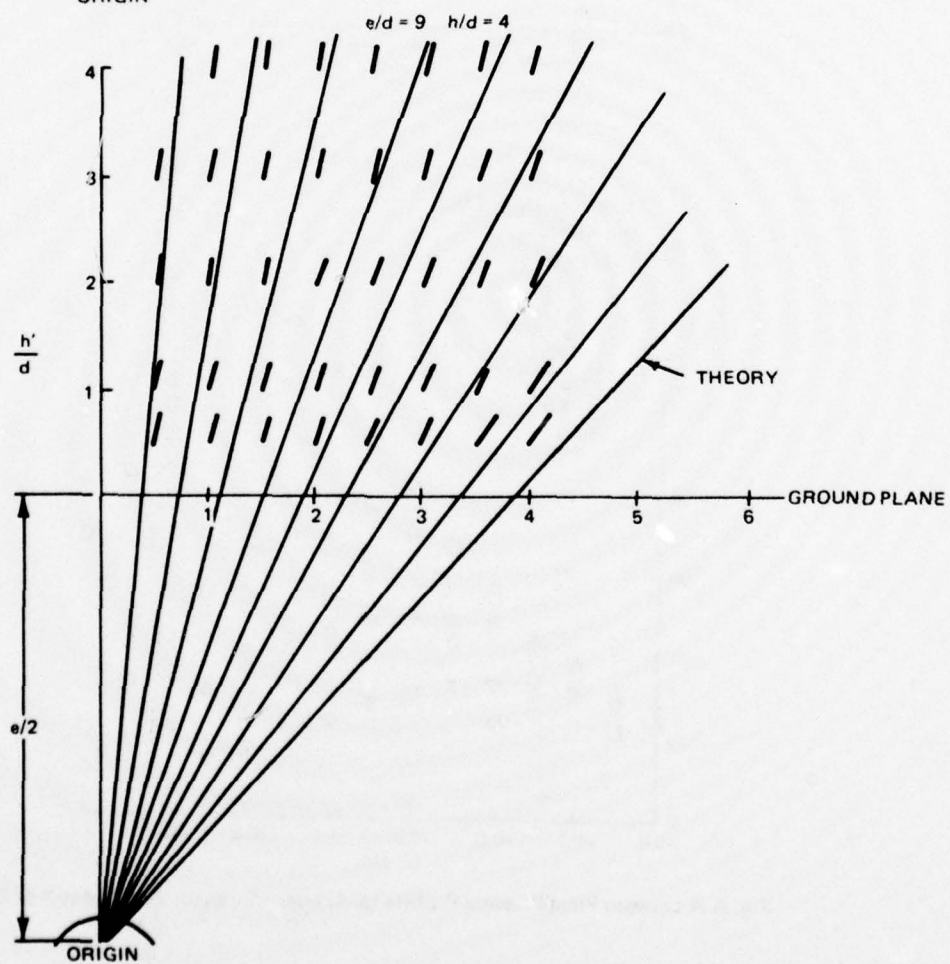Fig. A-5 Flow Direction in Upwash for Equal Strength Jets, Sheet 1 of 2
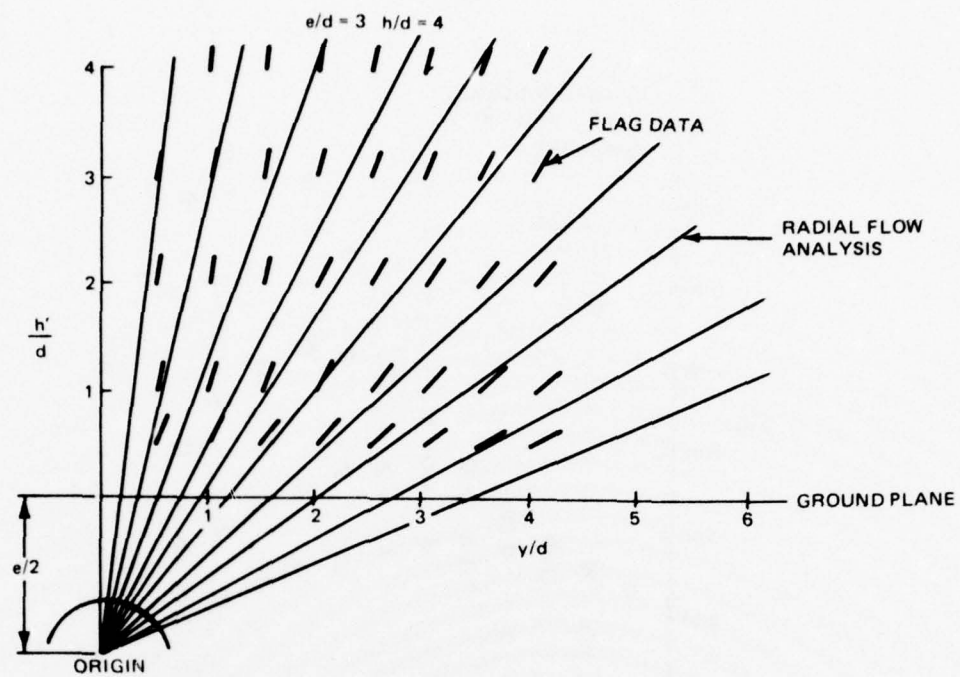
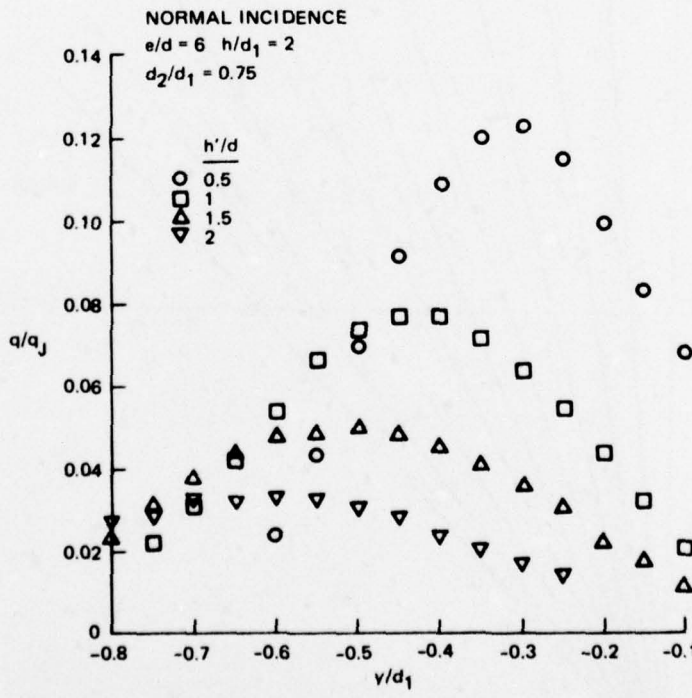Fig. A-5 Flow Direction in Upwash for Equal Strength Jets, Sheet 2 of 2
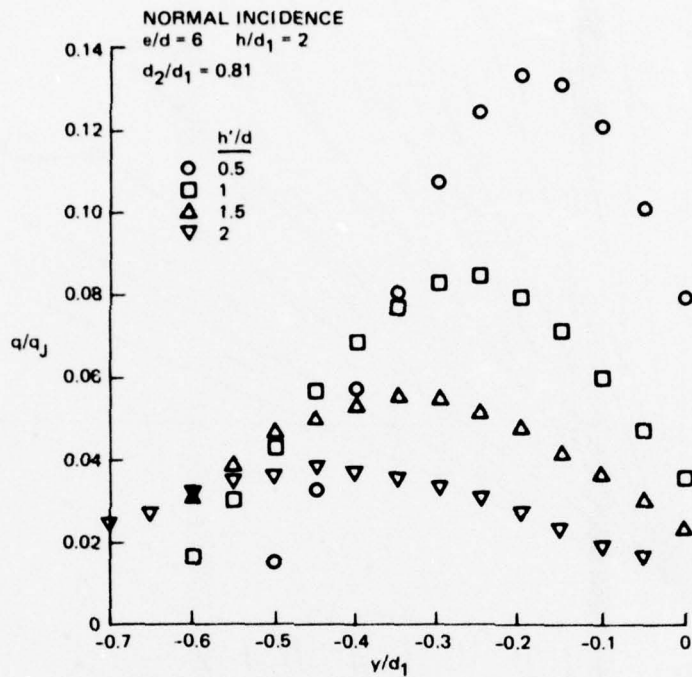
A-13

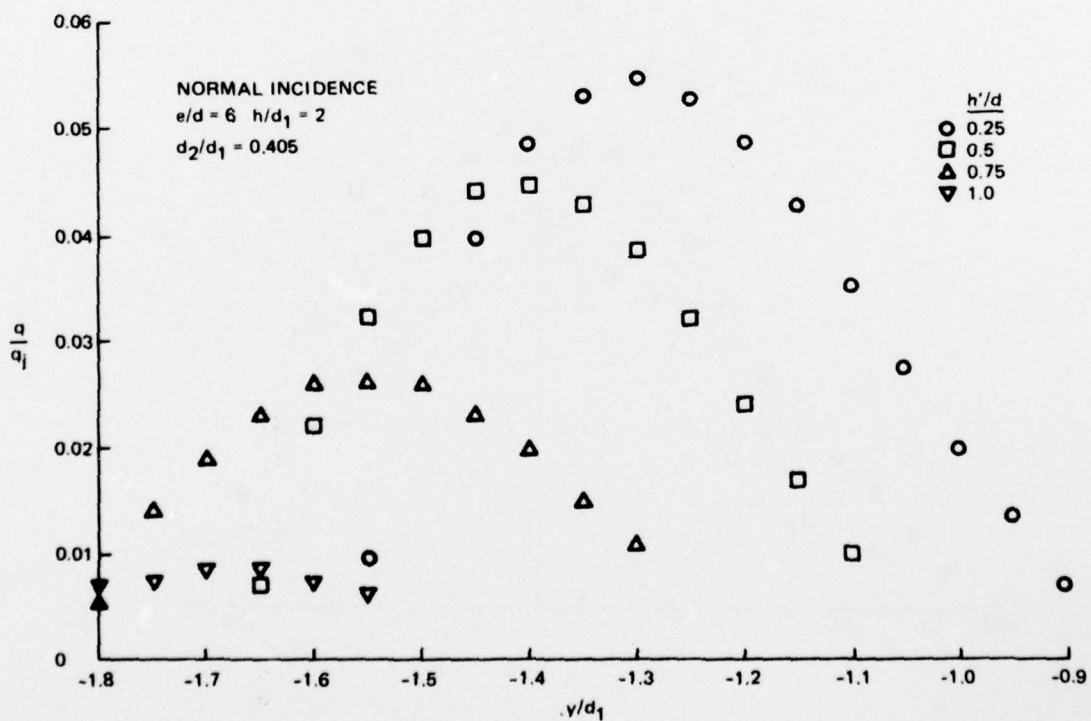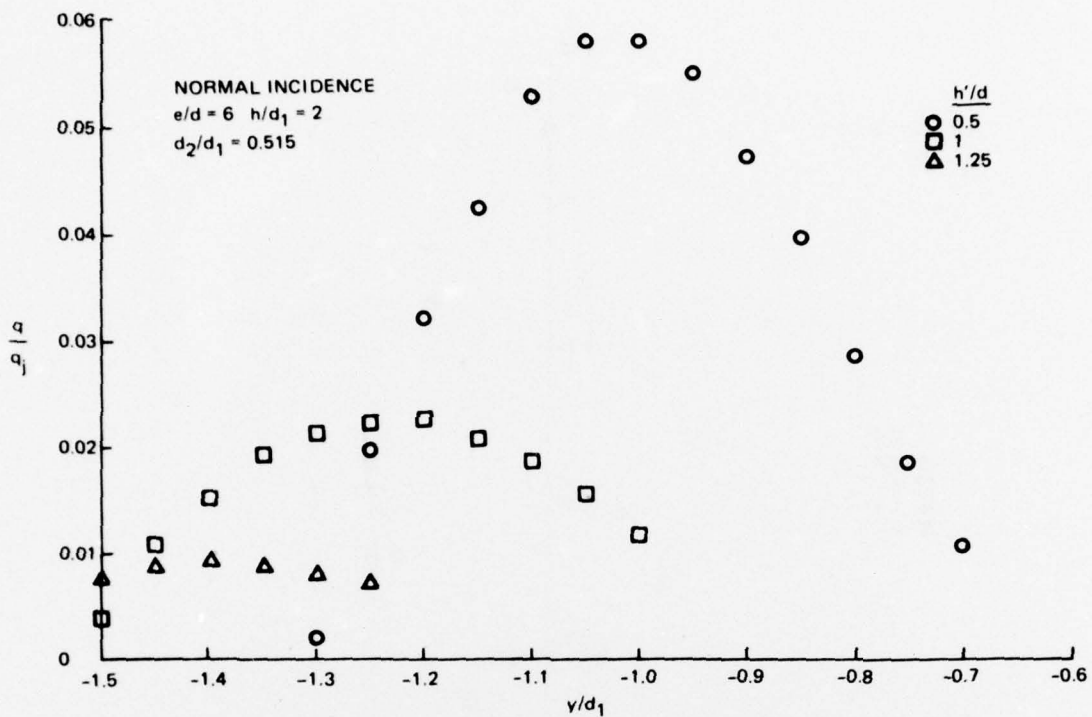Fig. A-6 Upwash Pitot Pressure Profiles for Unequal Strength Jets, Sheet 1 of 2

Fig. A-6 Upwash Pitot Pressure Profiles for Unequal Strength Jets, Sheet 2 of 2

Fig. A-7 Upwash Pitot Pressure Profiles for Equal Strength Inclined Jets, Sheet 1 of 5

Fig. A-7 Upwash Pitot Pressure Profiles for Equal Strength Inclined Jets, Sheet 2 of 5

A-17

Fig. A-7 Upwash Pitot Pressure Profiles for Equal Strength Inclined Jets, Sheet 3 of 5

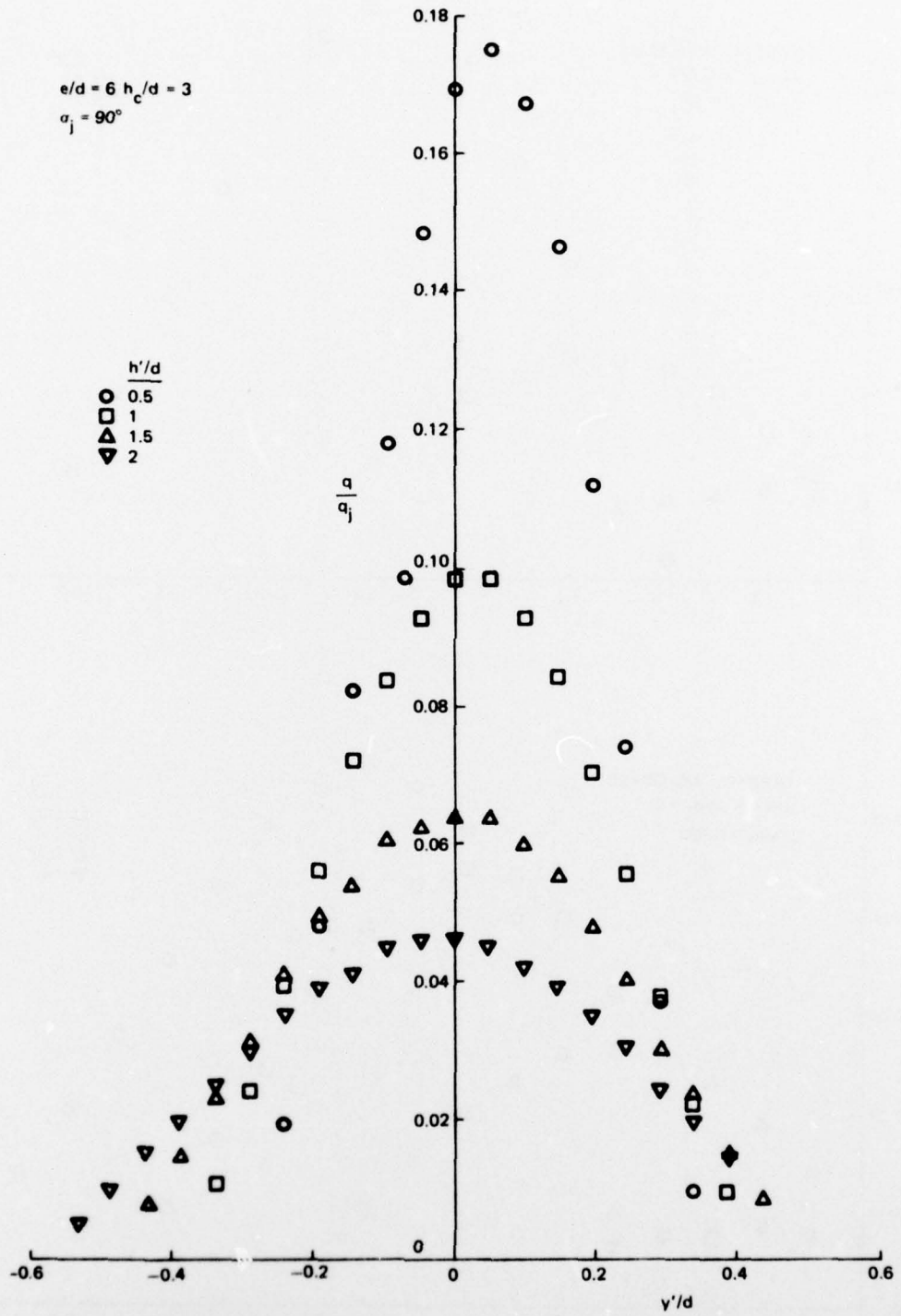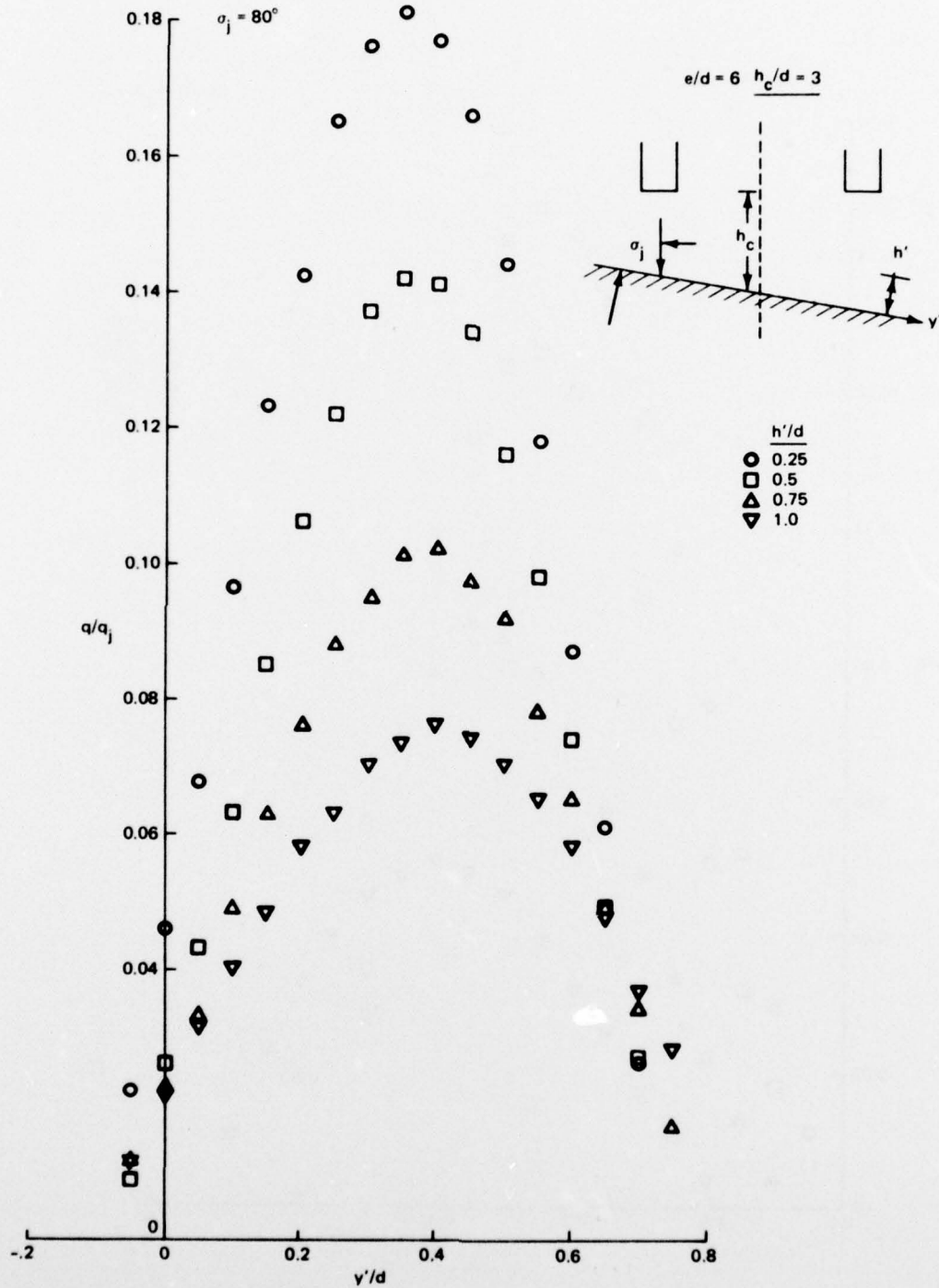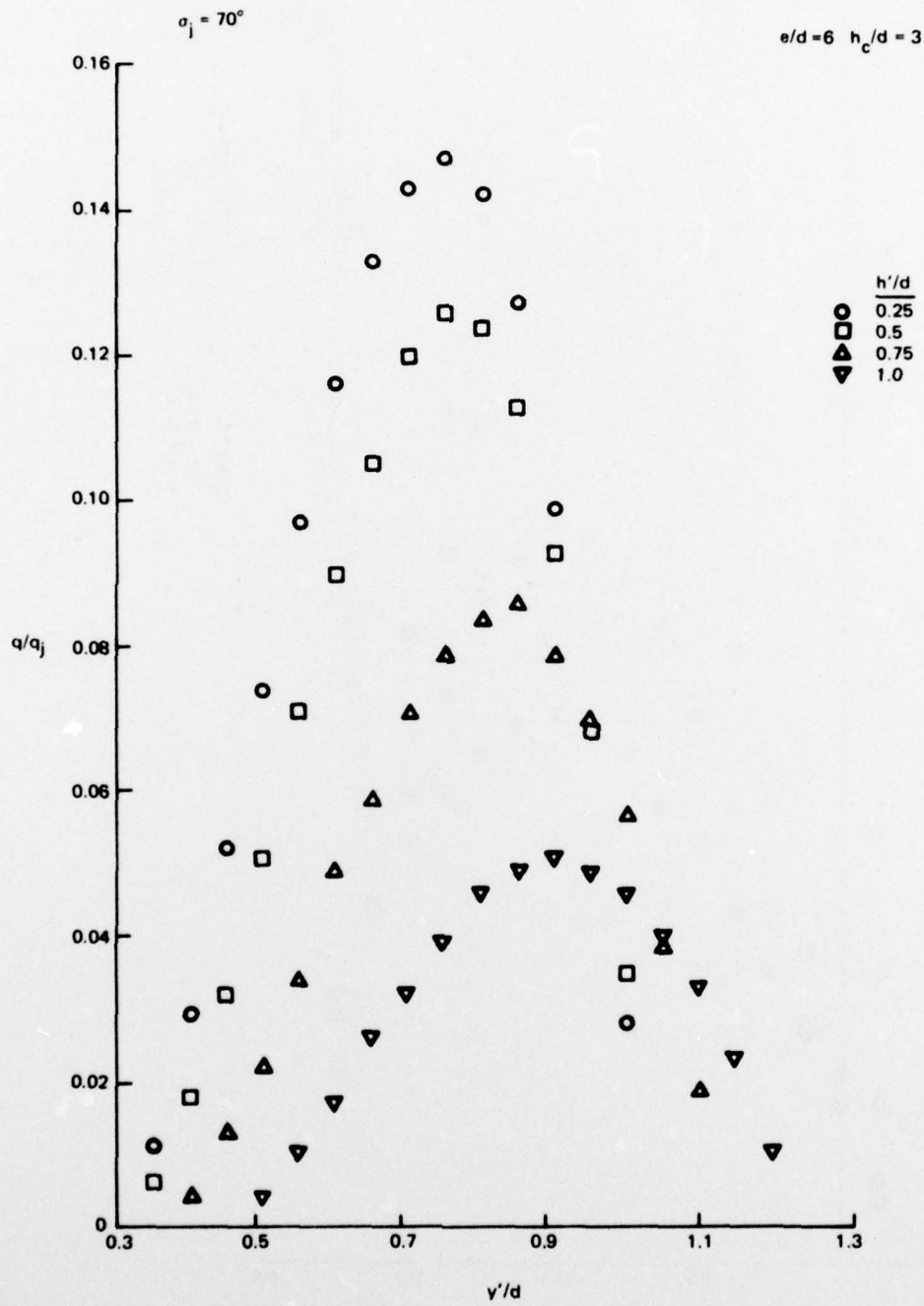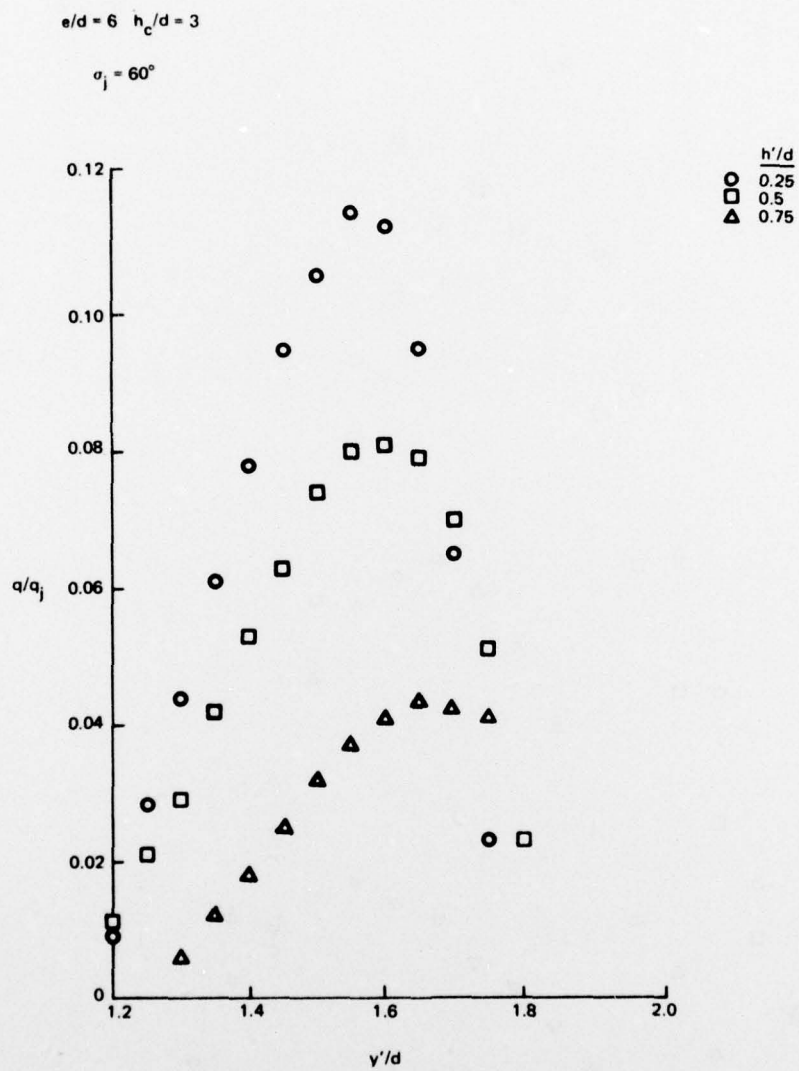e/d = 6 h_c/d = 3

σ_j = 60°

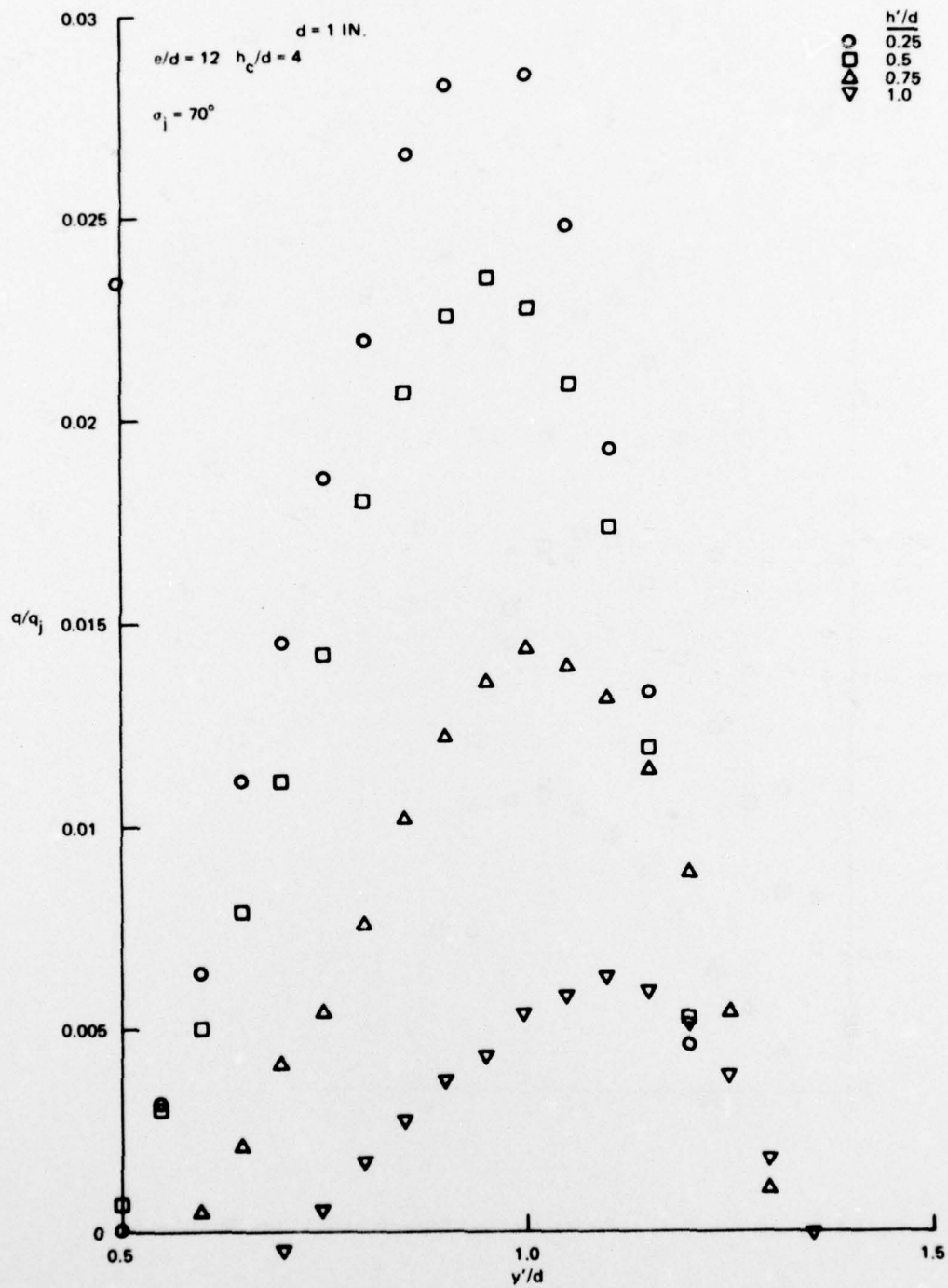Fig. A-7 Upwash Pitot Pressure Profiles for Equal Strength Inclined Jets, Sheet 4 of 5

Fig. A-7 Upwash Pitot Pressure Profiles for Equal Strength Inclined Jets, Sheet 5 of 5

APPENDIX B

MEASUREMENT TECHNIQUES IN UPWASH

For normal impingement of equal strength jets, the upwash forms a fan-shaped pattern that is directed normal to the ground plane. If the nozzles are spaced far enough apart, and if the ground plane is located within several diameters of the nozzle exit plane, the upwash fan passes between the shear layers of the incident jets. Providing there is no obstruction of the upwash flow near the nozzle exit plane (as would exist with flush-mounted jets emerging from an aircraft underside), the upwash has little if any influence on the incident jets. All of our experiments were run with no such obstruction in order to reduce fluctuations in local upwash properties to a tolerable level.

Even with the stabilizing restriction of no exit plane obstructions, the turbulence intensity was extremely high throughout the upwash and strongly affected by ground plane separation distance. Close ground plane spacing produced the lowest relative turbulence intensity level and hence the most accurately measureable upwash flows. However, even at $h/d = 2$, the local flow conditions in much of the region between the exit plane and the ground plane were essentially unsteady. In regions outside of the main upwash fan and the shear layers of the incident jets, we observed (using silk tuft probes) highly fluctuating flow angularity with complete velocity reversals occurring quite frequently.

Figure B-1 shows mean velocity profiles across the center-line of the upwash formed by normal impingement of equal strength jets. Two sets of data are displayed, one set taken with a hot film probe and one set with a pitot tube. Note that the data taken with these two different probes agree only in the central region of the upwash. Outside this region the pitot tube data provides a more realistic measurement of upwash velocity for reasons that are discussed below.

Figure B-2 shows a comparison between hot film and pitot tube
data for the same nozzle geometry with the ground plane located
at h/d = 6. These profiles show very poor agreement between
data taken throughout the upwash with the two different probes.
Oscilloscope traces showed that the fluctuation levels were much
higher while the mean velocities were much lower with the ground
plane further from the exit. Probing with a silk tuft showed
occasional velocity reversals even in the central region.

The increasingly poor agreement between hot film probe and
pitot probe data away from the central upwash region illustrates
a basic problem with hot film probes in highly fluctuating flow
fields. This problem can be visualized by considering a hot
film probe that is immersed in a one-dimensional fluctuating flow
in which the mean velocity is known to be zero. Time-averaging
hot film probe signals taken in such a hypothetical case would
yield a nonzero reading because the probe cannot distinguish
between forward and reverse flows; it would yield a positive
signal in either case. In essence, the probe would rectify the
velocity-time signal. By contrast, a pitot tube immersed in the
same hypothetical flow would provide a more accurate time-averaged
signal because it can yield negative signals when the flow over
the probe undergoes a local velocity reversal. While the pitot
tube cannot measure velocity accurately during a local flow
reversal (because the orifice is then in the wake of the probe),
it can yield negative signals which provide a better time-averaged
velocity than the hot film probe. These characteristics of signal
behavior were clearly observable in the upwash flow using oscilloscope
displays of both probe outputs before time-averaging.

This difference in signal response to fluctuating flow con-
ditions makes the pitot tube data more reliable in upwash measure-
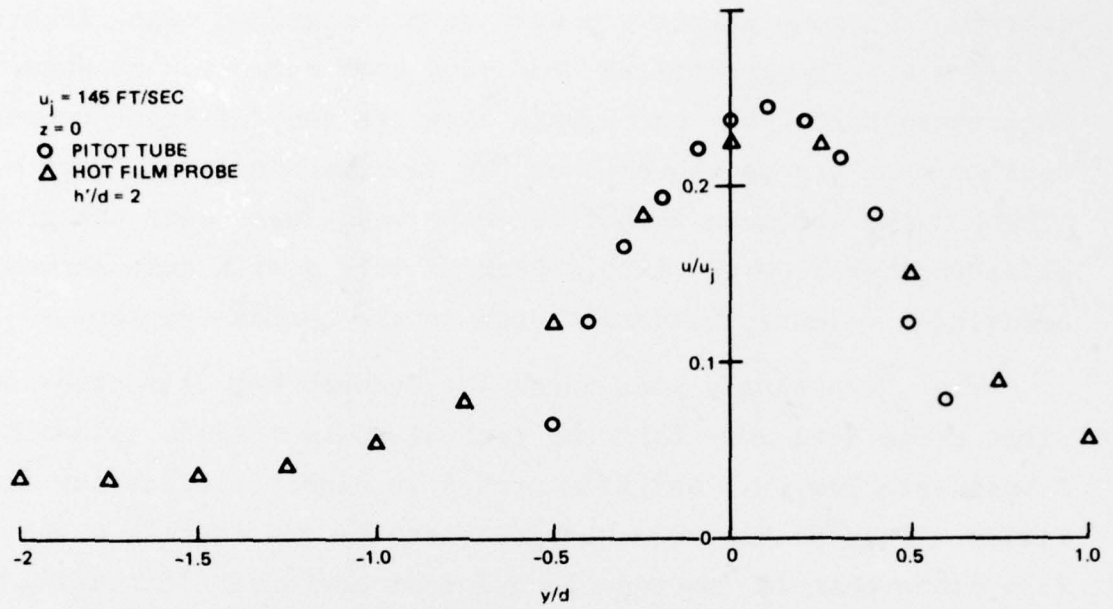ments since it can be used with confidence over a greater portion

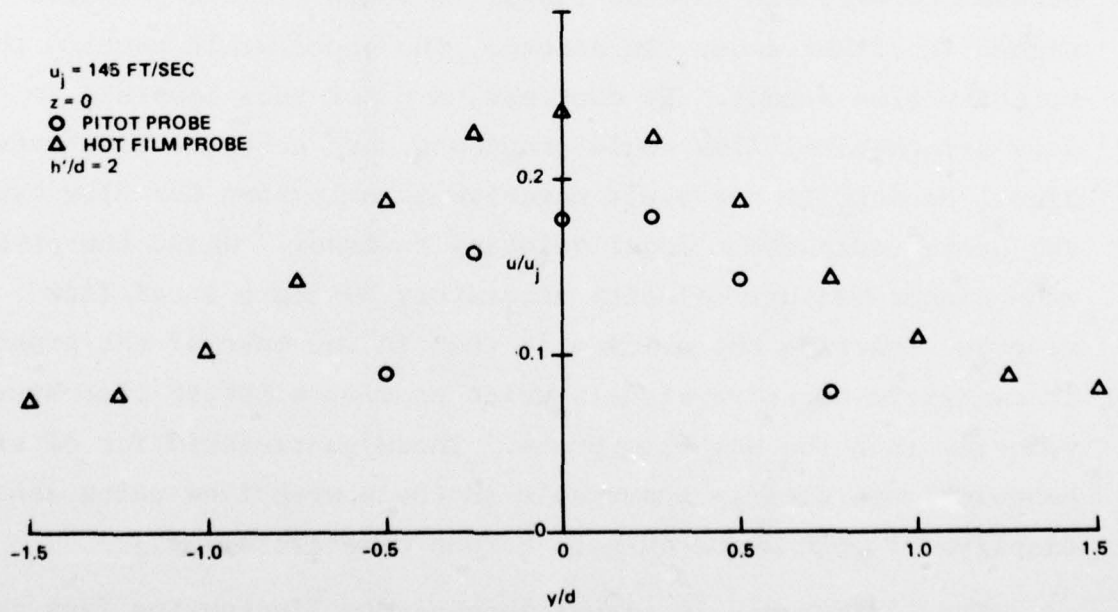Fig. B-1 Velocity Profiles Across Upwash with h/d = 2

Fig. B-2 Velocity Profiles Across Upwash with h/d = 6

of the flow field. Although the fast time response of the hot film probe makes it clearly superior for turbulence measurements, this advantage is essentially lost in upwash flows. Near the center of the upwash region we found $u'/u_J = 0.25$ while taking the data shown in Figure B-1. Since the turbulence level increased quite drastically away from the central region, and since $u'/u_J = 0.3$ is generally considered an upper limit for accurate measurements of turbulence intensity, we restricted the use of hot film probes and depended primarily on pitot tube data for most field surveys.

The increased turbulence intensity at greater ground plane spacing is partly attributable to a decreased local mean velocity in the upwash at large values of h/d. However the fluctuations also become stronger with a greater tendency toward local velocity reversal in the central upwash region as h/d increases. The latter effect may occur because the upwash is forced through an entrainment region bordering the shear layers that surround the incident jets, and these shear layers thicken toward the end of the core of the free stream flow.

In regions of the upwash that were free of local velocity reversals, measurements with a pitot probe were still subject to error because of fluctuations in local flow direction. Thin-wall tubing was used for the probes to minimize this source of error in mean velocity measurement. Figure B-3 shows calibration curves that were obtained for three probes that were immersed at different angles of incidence in a low-turbulence, uniform flow. The 1/8-inch-diameter pitot tube used for most of our work showed true total pressure up to about 20° misalignment with the flow. Keil probes were used in some of our work to help evaluate the effects of fluctuations of flow angularity on
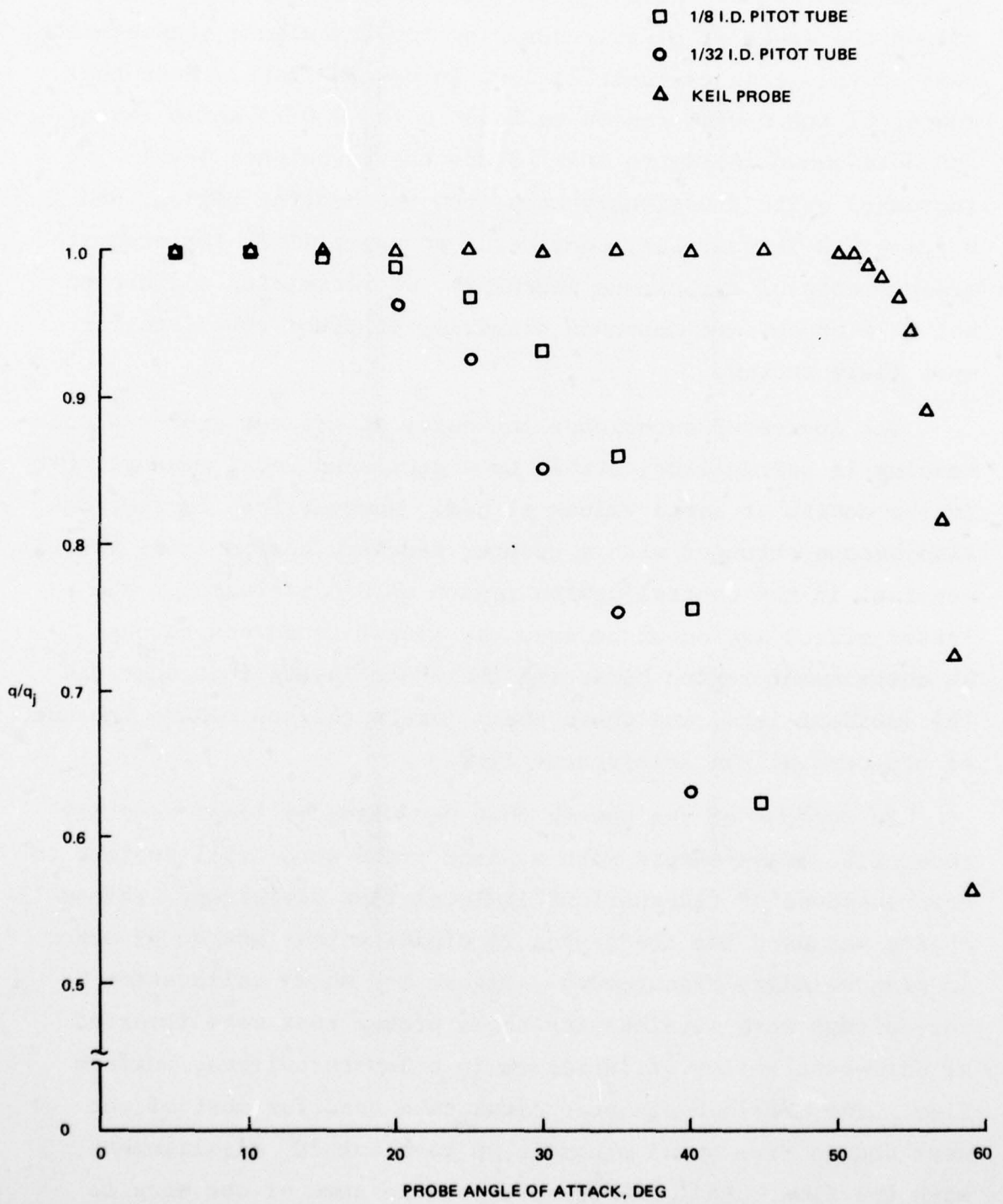
B-5

Fig. B-3 Angular Calibrations of Pressure Probes

time-averaged measurements. Orientation of the probe close to the expected mean flow direction helped to minimize errors cause by fluctuations in flow direction.

The mean flow direction in the upwash was found from our flag measurements to be close to the direction predicted by the radial flow model described in the text. As a check on this result we used two direction-sensitive hot film probes to measure local flow direction. One was an x-probe and the other a split-film probe. The x-probe consisted of two 0.006-inch-diameter cylindrical hot film sensors that were spaced 0.030 inches apart with their axes oriented at 90° with respect to each other. The split film probe consisted of a 0.006-inch-diameter cylindrical sensor on which two separate hot films were deposited, each film extending almost 180° around the sensor, with each film monitored by separate anemometer circuits. Both probes were calibrated for directional sensitivity as well as velocity using a 1/4 inch diameter nozzle fed by a throttled compressed air source. These probes were used to determine local flow direction and magnitude at a few points in the upwash for $e/d = 6$ and $h/d = 2$. Measurements were obtained with the x-probe located at $z = \pm 6$ inches for $h' = 1$, 2 and 3 inches. Following the procedure adopted with the flag measurements, the data taken at positive and negative z for the same h' were averaged. Measurements were obtained with the split film probe at values of z corresponding to the flag surveys at $h' = 1$ and 3 inches.

Table B-1 shows a comparison between probe measurements and data obtained from the flag array. Note that the flow angularity measured by both probes showed good agreement. The magnitude of the flow velocity measured by both probes also agreed and compared quite closely with the magnitude obtained by single

B-7

element hot film probes and pitot tubes in the central upwash.
Both probes indicate a somewhat greater flow inclination than
the flag measurements, although not enough greater to suggest
a significant discrepancy. Reasons for these differences could
be the distance over which the flags average measurements,
mutual interference between flags, or the optical method (long
duration exposure) used to obtain average inclination.

TABLE B-1 SUMMARY OF ANGULAR FLOW MEASUREMENTS IN UPWASH

| Z | $h' = 1$ inch | | | $h' = 3$ inches | | |
	Flags	Split Probe	x-Probe	Flags	Split Probe	x-Probe
1	10°	10°		11°	8°	
2	14	20		11	15	
3	22	29		17	21	
4	26	37		21	26	
5	33	44		27	31	
6	36	51	53°	29	36	38°
7	44	56		32	40	
8	51	59		32	44	

Measurements of flow inclination were more convenient with
the split film probe since it could be calibrated to measure
flow directions up to $\pm 90^{\circ}$ from the plane of the split. The x-
probe was limited to less than $\pm 45^{\circ}$ from the probe shaft, beyond
which ambiquity in the local flow direction invalidated measure-
ments, so the x-probe had to be re-aligned between measurements
in the inner and outer regions of the upwash. Because of its

greater range of flow angularity the split film probe should
provide more accurate time-averaged data in an environment
having large fluctuations in local flow direction. It should
be emphasized, however, that neither of these probes provides
an output that is linear with flow angle, and thus each would
display a different flow inclination if exposed to the same
fluctuations.